PD ST 0704
Restricted

Analytical Investigation of Supersonic Panel Flutter under Thermal Environment with Arbitrary Flow Direction

SOMENATH MUKHERJEE, DEEPA N, AVINASH R,
M MANJUPRASAD, S VISWANATH
Structures Division

Project Document ST 0704
March 2007

National Aerospace Laboratories
Bangalore 560 017, India

LIST OF SYMBOLS

a_{mn}	Amplitude coefficients
a	Panel length
b	Panel width
D	Panel stiffness, $\frac{Eh^3}{12(1-\mu^2)}$
E	Young's modulus
h	Panel thickness
μ	Poisson's ratio
w	Lateral deflection of panel
N_x , N_y , $N_{x\,y}$	Midplane stress resultants
N_{xo} , $N_{y\,o}$,	Midplane uniform stress resultants
N_{xT}, N_{yT} , $N_{x\,yT}$	Midplane thermal stress resultants
γ	Mass density of panel
p	Aerodynamic pressure load per unit area
M	Mach number
q	$\frac{\rho_{air} v^2}{2}$ Dynamic pressure
ρ_{air}	Air density
v	Velocity of airflow
v_s	Velocity of sound
ϕ	Airy stress function
T	Temperature
ΔT_1	Difference of temperature between center and edges of parabolic temperature distribution
ΔT_2	Difference between ambient and reference temperature
α	Coefficient of thermal expansion
Ω	Generalized eigenvalue

ω	Frequency
m,n,r,s	integers
x, y, z	Cartesian coordinates of panel
R	total no of terms in flow direction
S	total no of terms in cross-flow direction
t	time

$$c = -\frac{6\left[1+\left(\frac{a}{b}\right)^2\right]}{1+\frac{4}{7}\left(\frac{a}{b}\right)^2+\left(\frac{a}{b}\right)^4}$$

$\lambda = \frac{2qa^3}{D\sqrt{M^2-1}}$ Dynamic pressure parameter

λ_{cr} Critical value of λ

$k^2 = \frac{\gamma h a^4}{\pi^4 D}\omega^2$ Frequency parameter

$\psi = \frac{\alpha E h a^2 \Delta T_1}{\pi^2 D}$ Thermal stress parameter

$R_{xo} = \frac{N_{xo} a^2}{\pi^2 D}$ Edge load parameter (x-direction)

$R_{yo} = \frac{N_{yo} a^2}{\pi^2 D}$ Edge load parameter (y-direction)

Notation,

$$\nabla^2 = \frac{\partial^2}{\partial x^2} + \frac{\partial^2}{\partial y^2}$$

$$\nabla^4 = \frac{\partial^4}{\partial x^4} + 2\frac{\partial^4}{\partial x^2 \partial y^2} + \frac{\partial^4}{\partial y^4}$$

CONTENTS

CHAPTER 1

INTRODUCTION

1.1 Introduction to Aeroelasticity

Aeroelasticity is the study of the effect of aerodynamic forces on elastic bodies. Aeroelasticity includes certain phenomena involving mutual interaction among inertial, aerodynamic and elastic forces.

The classical theory of elasticity deals with the stress and deformation of an elastic body under prescribed external forces and displacements. The external loading acting on the body is, in general, independent of the deformation of the body. It is usually assumed that the deformation is small and does not substantially affect the action of external forces. In such a case we often neglect the change in dimensions of the body and base our calculation on the initial shape. The situation is different, however, in most significant problems of aeroelasticity. The aerodynamic forces depend critically on the attitude of the body relative to the flow. The elastic deformation plays an important role in determining the external loading itself. The magnitude of the aerodynamic force is not known until the elastic deformation is determined.

One of the interesting problems in aeroelasticity is the stability (or rather instability) of a structure in wind. For a given configuration of the elastic body, the aerodynamic force increases rapidly with the wind speed, while the elastic stiffness is independent of the wind, there may exist a critical wind speed at which the structure becomes unstable. Such instability may cause excessive deformations, and may lead to the destruction of the structure.

1.2. Aeroelastic Phenomena

Aeroelastic problems would not exist if airplane structures were perfectly rigid. Modern airplane structures are very flexible, and this flexibility is fundamentally responsible for the various types of aeroelastic phenomena. There are several aeroelastic phenomena involving interaction among aerodynamic, inertial and elastic forces.

Fig 1.1 classified the problems in aeroelasticity by means of a triangle of forces. Based upon the interaction between the three forces the aeroelastic problems can be classified as

i. **Dynamic aeroelastic problems**
ii. **Static aeroelastic problems**

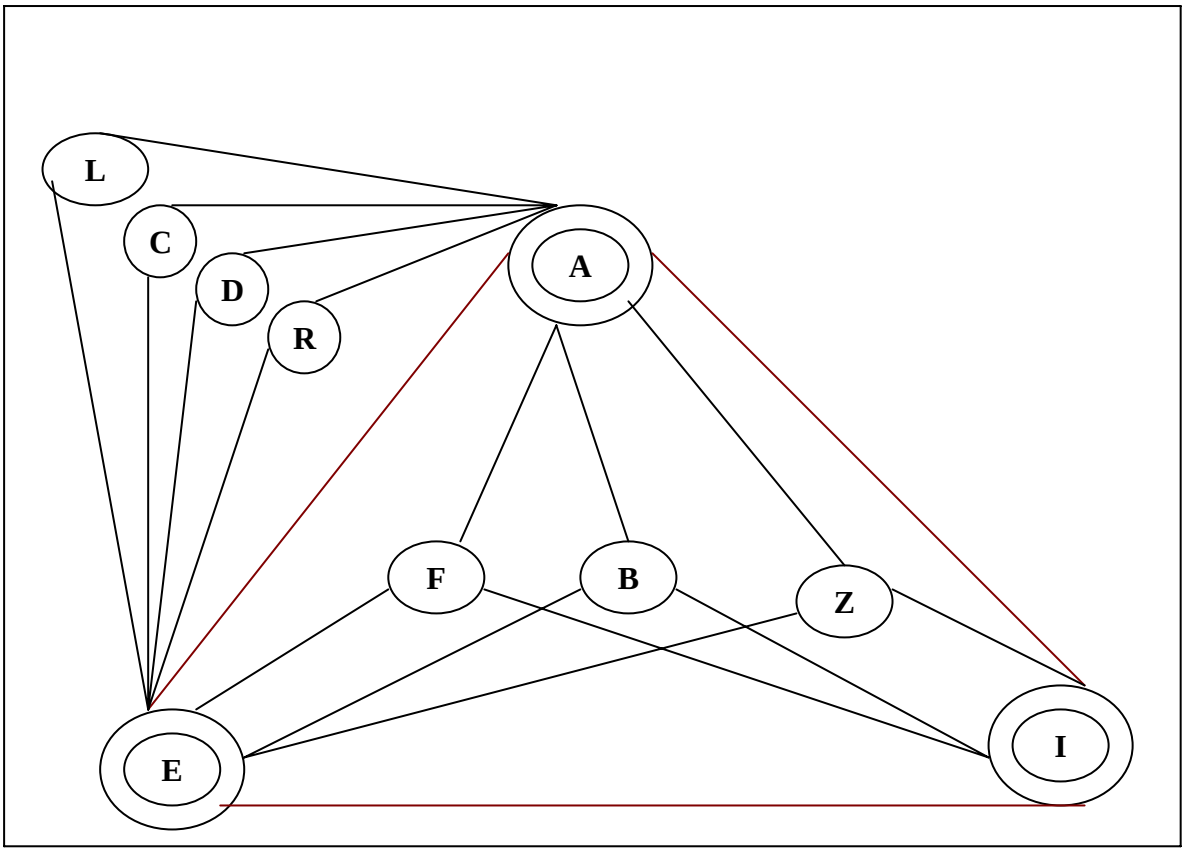

Fig 1.1. Aeroelastic phenomena

A-Aerodynamic force
E-Elastic force
I- inertial force

<u>Dynamic Aeroelastic problem:</u>
F-Flutter
B-Buffeting
Z-Dynamic Response
<u>Static Aeroelastic problems:</u>
L-Load Distribution
C-Control Effectiveness
D-Divergence
R-Control System Reversal

The three types of forces aerodynamic, elastic and inertial represented by symbols A, E, I respectively are placed at the vertices of an equilateral triangle. Each aero-elastic phenomenon can be located in Fig 1.1 and classified according to its relation to the three vertices. Thus the static aero-elastic phenomena from A and E lie outside the triangle on the upper left side, whereas dynamic aero-elastic phenomena lie within the triangle, since they involve all three kinds of forces.

Flutter (**F**):

A dynamic instability occurring in an aircraft in flight, at a speed called flutter speed, where the elasticity of the structure plays an essential part in the instability

Buffeting (**B**):

Transient vibration of aircraft structural components due to aerodynamic impulses produced by the wake behind wings, nacelles, fuselage pods, or other components of the airplane.

Dynamic response (**Z**):

Transient vibration of aircraft structural components produced by rapidly applied loads due to gusts, landing, gun reaction, abrupt control motions, moving shock waves, or other dynamic loads

.

Load distribution (**L**):

Influence of elastic deformations of the structure on the distribution of aerodynamic pressures over the structure.

Control Effectiveness (**C**):

Influence of elastic deformations of the structure on the controllability of an airplane.

Divergence (**D**):

A static instability of a lifting surface of an aircraft in flight, at a speed called the divergence speed, where the elasticity of the lifting surface plays an essential role in the instability.

Control system reversal (**R**):

A condition occurring in flight, at a speed called the control reversal speed, at which the intended effects of displacing a given component of the control system are completely nullified by elastic deformations of the structure.

1.3. Flutter- An Introduction to Dynamic Aeroelasticity

The most dramatic physical phenomenon in the field of aeroelasticity is flutter; a dynamic instability often leads to catastrophic structural failure. Flutter has the most far-reaching effects of all aeroelastic phenomena on the design of high-speed aircraft. Flutter can be defined as the dynamic instability of an elastic body in an air stream. It is most commonly encountered on bodies subjected to large lateral aerodynamic loads of the lift type, such as aircraft wings, tails and control surfaces.

To describe the physical phenomenon, consider a cantilever wing mounted in a wind tunnel (a chamber in which air is forced at control velocity in order to study the effect of aerodynamic flow over the elastic structure) at a small angle of attack and with a rigid support at the root. When there is no flow in the wind tunnel, and the model is disturbed oscillation sets in, which is damped gradually. The amplitude of oscillations decreases with time as shown in Fig.1.2.a When the speed of flow in the wind tunnel gradually increases, the rate of damping of the oscillation of the disturbed airfoil first increases, with further increase of the speed of flow, however a point is reached at which the damping rapidly decreases. At the critical flutter speed, an oscillation can just maintain itself with steady amplitude as shown in Fig.1.2 .b. At speeds of flow somewhat above the critical, the amplitude of the oscillations will increase with time as shown in Fig.1.2.c. In such circumstances the airfoil suffers from oscillatory instability and is said to be flutter.

Flutter can be defined as self-sustained oscillation that can maintain itself with steady oscillation i.e. without any external oscillator or forcing agency. The flutter problem is one of dynamic stability of the structure in an airflow, and reduces to finding

the (critical) speed at which small disturbances will take the structure out of dynamic stability, or, more precisely, that speed which, when exceeded, will result in small disturbances causing increasing self-excited oscillations. The avoidance of flutter is always a main requirement in aircraft design.

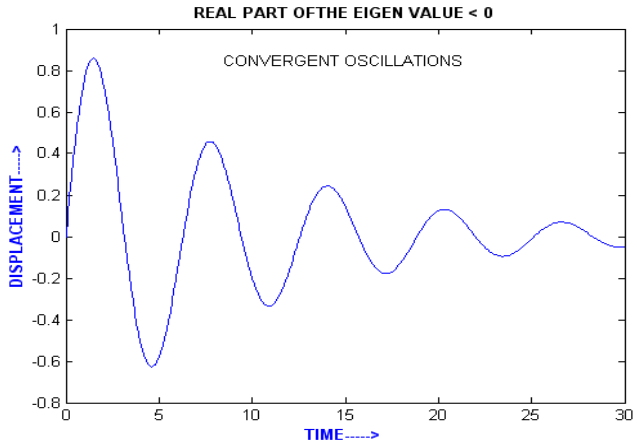

Fig.1.2. (a) Stable ($v<v_{cr}$)

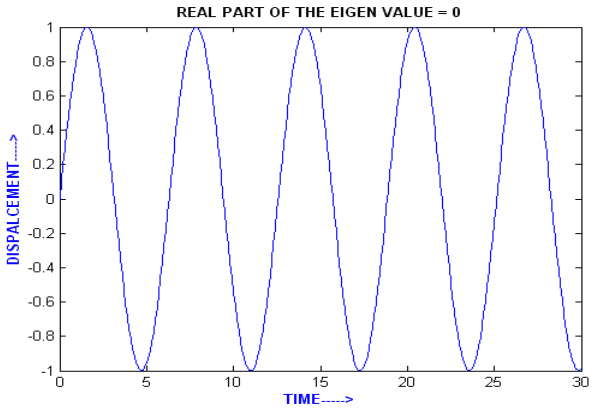

Fig.1.2. (b) Flutter boundary ($v=v_{cr}$)

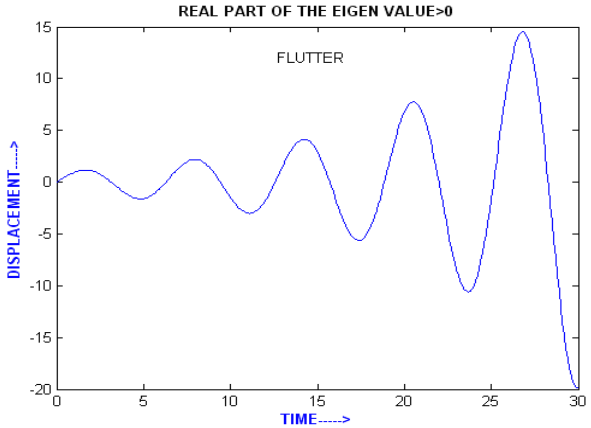

Fig.1.2. (c) Unstable, Flutter ($v>v_{cr}$)

1.4. Supersonic Panel Flutter

The aircraft of today have evolved into complex flying machines that can achieve challenging tasks while flying at enormous speeds in the supersonic and hypersonic regimes. A typical fighter jet can fly at about Mach 5, while a re-entry vehicle can reach speeds of about Mach 12.

At very high speed of flight, the skins of an airframe may exhibit flutter, in which the degrees of freedoms are those associated with displacement of the panel in a direction normal to its surface. This is called panel flutter and it differs from the more conventional lifting surface flutter in at least two important aspects: first, it is entirely a supersonic phenomenon, and second, structural non-linearities associated with aerodynamic boundary layer effects tend strongly to limit the flutter amplitudes.

Panel flutter is a self-excited oscillation of the external surface skin of a flight vehicle, which results from the dynamic instability of the aerodynamic, inertial, and elastic forces of the system.

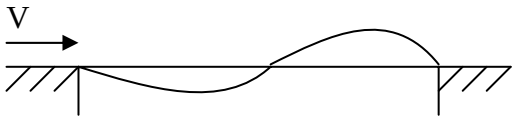

Fig 1.3. Deformation of a two-dimensional panel

Consider a flat plate, which spans on two rigidly supported edges, as shown in Fig1.3. Let the air flow over one side of the plate and remain stagnant on the other side. In supersonic flow, a type of self-excited oscillation may occur in certain ranges of critical dynamic pressure, whose value depends on the initial curvature and the stiffness of the plate, the ratio of the density of air to that of the plate, the dimensions of the plate, and the thrust exerted by the supports at the edges of the plate. This is called panel flutter.

One of the practical causes of panel flutter is the thermal stress induced in the skin due to aerodynamic heating in flight at high speeds. If the skin is hotter than the supporting structures, compressive stress may be induced in the skin. If the temperature difference between the supporting structures and the skin is sufficiently large, the skin may become buckled. A buckled skin has a much lower critical dynamic pressure than an unbuckled one.

The most practical method of preventing panel flutter is to introduce tension into skin, for example, by internally pressurizing the wing or fuselage.

1.5. Literature Review

Excellent treatises on the classical theory of aeroelasticity have been presented by Fung [1], Bisplinghoff and Ashley [2]. The physics and computational aspects of various kinds of static and dynamic aeroelastic problems have been highlighted. The earliest study of flutter seems to have been made by Lanchester [3], Bairstow and Fage [4] in 1916 in connection with the anti symmetrical (fuselage torsion-elevator torsion) flutter of a Handleg Page Bomber. Up to 1934, only a few cases of flutter were recorded. In those

days only airplane wings showed flutter. Aileron mass unbalance and low torsional stiffness of the wing were responsible for most of these accidents.

The aeroelastic instability of aircraft skin panels has been the subject of a number of theoretical investigations. During the second world war of 1939-1945, Germany launched a number of V2 missiles. Many of these missiles failed during flight, the cause of which was later recognized as supersonic flutter of the missile fins [5]. In his analysis of supersonic flutter, Ashley developed a simple mathematical formula, based on a theory called the "Piston Theory" to estimate the aerodynamic loads for supersonic flow. In the early part of world war, most of the flutter cases were due to insufficient aileron mass balance and most tail-surface flutter cases were due to control surface tabs. Towards the latter part of world war, airplane speed increased towards the transonic range, and supersonic missiles appeared.

Early experimental and theoretical studies of the flutter behavior of buckled plates were carried out by Fung [6]. The primary concern was with the prediction of stability boundaries, although Fung did derive modal equations of motion for finite amplitude motions of the plate. Herman and Sidney [7] have compared experimental results with the theoretical predictions of panel flutter, and have concluded that the linearized, quasi-steady aerodynamic theory is valid only beyond Mach 1.3.

Stability boundaries for buckled two-dimensional plate were calculated by Hedgepeth [8] using an approach similar to Fung-Hedgepeth's application of the two-dimensional static aerodynamic approximation to the panel flutter problem. It greatly simplified the analytical complexities and resulted in a differential equation that can be solved exactly for finite panels. It has shown that a system of uniform stresses can greatly reduce the flutter speed of an unbuckled panel. During 1950's, several experimental investigations were conducted to verify the existence of panel flutter and to determine some of the effect of such parameters as panel length-width ratio, thickness, and differential pressure.

The effect of buckling on flutter boundaries of three-dimensional plates was investigated by Fralich [9]. He used Von Karman large deflection plate equations and Ackeret's expression for the aerodynamic pressure. The equations were transformed into pair of nonlinear ordinary differential equation by Galerkin's method, using the first two modes of a simply supported plate as coordinate function. A stability analysis is carried out for each buckling load by linearizing these equations about the buckled configuration, and computing the eigenvalues in the usual manner.

In many problems of panel flutter the most obvious methods of analysis have been to apply the Galerkin's method using the governing equations of the problem. The applicability of the Galerkin's method to the supersonic membrane flutter problem has been studied by Ellen [10] and found to give good agreement with exact solutions. Sander *et al* [11] have employed the finite element method for supersonic flutter analysis using a new conforming quadrilateral (CQ) element.

Using piston theory and analytical methods, Harry and Walter [12] had reported the results of their investigation for the flutter behaviour of simply supported, thermally stressed square panel subjected to supersonic airflow along one edge of the panel.

Erickson [13] has also reported the results of panel flutter investigation for orthotropic panels.

1.6. Objectives and Summary of the present work

The objective of present work is to investigate the effects on the flutter boundary of rectangular panels from both flow directions and aspect ratio, in addition to those from thermal conditions (associated with a parabolic temperature profile). The work presented in reference [12] for flow along the panel edges have been extended for generating flutter boundaries for panels subjected to *arbitrary* flow directions. Furthermore, the effect of edge loading from the in-plane edge constraints to thermal expansion at the supports has also been a topic of investigation. The aerodynamic forces from the supersonic airflow have been modeled using piston theory aerodynamics [5].

This investigation has been initiated to provide a theoretical basis for the estimation of the flutter boundaries of the various structural panels of the Re-usuable Launch Vehicle (RLV).

The report begins with an introduction to aeroelasticity and aeroelastic problems related to launch vehicles. In Chapter 2, the analytical formulation for supersonic panel flutter analysis of the flat simply supported rectangular plate is dealt with. Linearized quasi-steady two-dimensional aerodynamic (piston theory) is used in conjunction with thin-plate theory to formulate the problem. The panel is subjected to supersonic airflow in arbitrary direction and is associated with a parabolic temperature distribution over the plate. The solution for the equation is obtained using Galerkin's procedure.

In Chapter 3, the supersonic panel flutter analysis of rectangular panels without thermal effects is dealt with. The critical dynamic pressure parameter that leads to flutter for panels of various aspect ratios and different flow direction is determined. In Chapter 4, the adverse thermal effect on supersonic flutter boundary due to parabolic temperature distribution over the panel and in-plane edge loading from in-plane constraints is presented. The results are generated for various aspect ratios and flow direction.

Numerical studies have been carried out for panels of various aspect ratios and results are presented in Chapter 5. The variation of critical parameters (dynamic pressure/ velocity) due to the in-plane edge loading from in-plane constraints and parabolic temperature distribution over the panel is generated using the analytical method. The results are validated with the commercial finite element software **NASTRAN** wherever possible. Good agreement between the results can be observed.

CHAPTER 2

MATHEMATICAL FORMULATION FOR SUPERSONIC PANEL FLUTTER

2.1 Problem summary:

The problem of panel flutter of a plate, simply supported on all edges, subjected to supersonic airflow in arbitrary direction is treated theoretically. The effect of self-equilibrating stress state associated with a parabolic temperature distribution is also included in the flutter analysis. Linearized, quasi-steady, two-dimensional aerodynamics is used in conjunction with thin-plate theory to formulate the problem. The solution for the equation is obtained using Galerkin's procedure.

2.2 Formulation:

2.2.1 Statement of problem

The configuration to be analyzed herein is shown in Fig 2.1. It consists of a flat rectangular panel of length '*a*', width '*b*', and uniform thickness '*h*'. The panel is simply supported on all edges. It is subjected to a supersonic airflow at Mach number '*M*' along the direction making an angle 'θ' with the edge '*a*' of the panel.

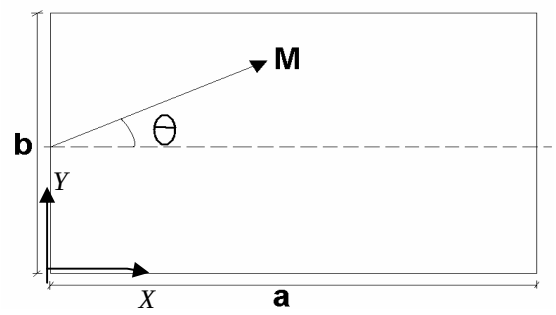

Fig 2.1 Panel under flow along the direction making an angle 'θ' with the edge '*a*' of the panel.

The panel is subjected to a parabolic temperature distribution in the middle plane as in Fig 2.2, with temperature difference of *ΔT1* between the center and the edges. The parabolic temperature distribution over the panel is given mathematically by the function

$$T(x,y) = 16\Delta T_1\left(\frac{x}{a}\right)\left(1-\frac{x}{a}\right)\left(\frac{y}{b}\right)\left(1-\frac{y}{b}\right) \qquad (2.1)$$

where the rise in temperature at the panel center with respect to that at the edges is given by $\Delta T_1 = T_{center} - T_{edges}$.

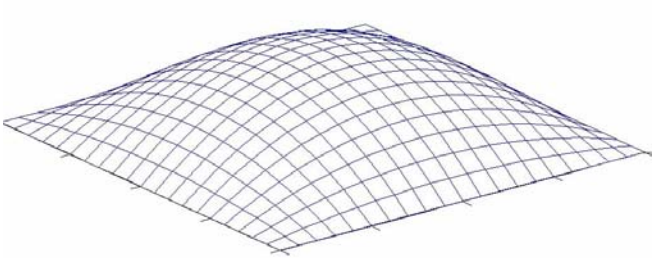

Fig 2.2 Parabolic Temperature Distribution over the Panel.

Uniform edge loading per unit edge lenght N_{xo} and N_{yo}, may be applied at the boundaries to account for the *(i)* Movable edge supports *and / or (ii)* In-plane edge constraints to thermal expansion at the immovable supports (instead of simply supported ends) due to the difference of ambient temperature from the reference temperature. Panels with immovable hinged supports at all edges can develop such in-plane loadings due to thermal conditions. A more detailed discussion of this aspect is presented in Article 2.3.

A schematic view of a panel subjected to airflow along *x*-direction ($\theta = 0$) and edge loads N_{xo} and N_{yo} at the boundaries is presented in Fig 2.3.

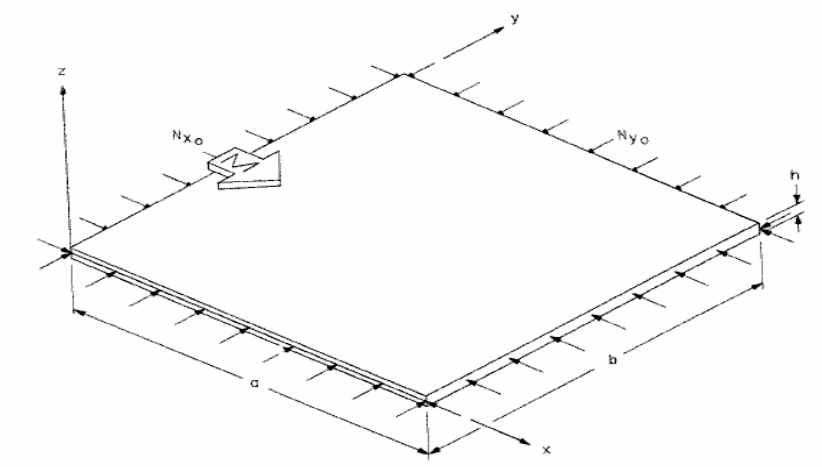

Fig 2.3 Panel subjected to airflow along x-direction

2.2.2 Basic equations

The equation of motion of the panel under a loading per unit area is given as

$$D\nabla^4 w + N_x \frac{\partial^2 w}{\partial x^2} + 2N_{xy} \frac{\partial^2 w}{\partial x \partial y} + N_y \frac{\partial^2 w}{\partial y^2} + \rho_{mat} h \frac{\partial^2 w}{\partial t^2} = p \qquad (2.2)$$

Here *w* is the transverse displacement (due to dynamic pressure) which is a function of *x*, *y* and tine *t*, $D = \frac{Eh^3}{12(1-\mu^2)}$ is flexural rigidity of the panel, *E* is the materials Young's modulus, μ is the Poisson's ratio and *h* is the thickness of the plate. The net *in-plane* loading (assumed positive for compression) per unit width along *x*- and *y*-directions of the panel are given by N_x and N_y respectively. The mass per unit area of the panel is $\rho_{mat} h$, (ρ_{mat} = mass density of the panel material).

The aerodynamic pressure load p is obtained by use of linearized, quasi-steady, two-dimensional aerodynamics (Piston theory). Piston theory is a useful tool for calculating the aerodynamic forces on a surface by obtaining a point function relationship between the local pressure generated on the surface and the local normal component of fluid velocity at the surface, in the same way that these quantities are related at the face of a piston moving in a one-dimensional channel. Essentially the forces so calculated are static forces.

$$p = \frac{-2q}{\sqrt{M^2-1}}\frac{\partial w}{\partial x}\cos\theta + \frac{-2q}{\sqrt{M^2-1}}\frac{\partial w}{\partial y}\sin\theta \tag{2.3}$$

Here *q* is the dynamic pressure ($q=\rho_{air} V^2/2$) and *M* is the Mach number ($M=V/V_{sound}$). The net mid-plane force intensity terms in equation (2.2) is written as the sum of those induced by applied, uniform, normal forces at the boundary and those resulting from the parabolic temperature distribution as follows:

$$\begin{aligned} N_x &= N_{xo} + N_{xT} \\ N_y &= N_{yo} + N_{yT} \\ N_{xy} &= N_{xyT} \end{aligned} \tag{2.4}$$

We first consider the thermal contributions from the parabolic tempertuare distribution only, so that the components $N_{xo} = N_{yo} = 0$. For the parabolic temperature profile alone, the thermally induced stress resultants vanish at the boundaries that do not offer any constraints to thermal expansion. These are determined in terms of stress function $\phi = \phi(x, y)$ from the following relationships,

$$\begin{aligned} N_{xT} &= \frac{\partial^2 \phi}{\partial y^2} \\ N_{yT} &= \frac{\partial^2 \phi}{\partial x^2} \\ N_{xyT} &= -\frac{\partial^2 \phi}{\partial x \partial y} \end{aligned} \tag{2.5}$$

Assume a stress function of the form

$$\phi = C\alpha E h a^2 \Delta T_1 \left(\frac{x}{a}\right)^2 \left(\frac{x}{a}-1\right)^2 \left(\frac{y}{b}\right)^2 \left(\frac{y}{b}-1\right)^2 \tag{2.6}$$

where α is the thermal coefficient of linear expansion of the panel material, and C is a constant, to be determined from the edge conditions.
The condition that the panel be free from thermally induced in-plane normal and shear stresses on the boundaries (due to parabolic temperature alone) requires that the stress function satisfy the following boundary conditions. For the purpose of this analysis the panel is considered to be simply supported against the lateral deflections, but unrestrained to in-plane displacements at the boundaries.

$$\begin{aligned}&\phi(0,y)=\phi(a,y)=\phi(x,0)=\phi(x,b)=0\\&\frac{\partial\phi}{\partial x}(0,y)=\frac{\partial\phi}{\partial x}(a,y)=\frac{\partial\phi}{\partial y}(x,0)=\frac{\partial\phi}{\partial y}(x,b)=0\end{aligned} \tag{2.7}$$

For compatibility of in-plane strains, the stress function must satisfy the following partial differential equation.

$$\nabla^4\phi=\alpha Eh\nabla^2 T \tag{2.8}$$

Applying Galerkin's technique to equation (2.8), one can express the constant C as

$$C=-\frac{6\left[1+\left(\frac{a}{b}\right)^2\right]}{1+\frac{4}{7}\left(\frac{a}{b}\right)^2+\left(\frac{a}{b}\right)^4} \tag{2.9}$$

Thus the in-plane stress resultants (force per unit length) from the parabolic thermal profile are given from equations (2.5) as

$$N_{xT}=C\alpha Eha^2\Delta T_1\left(\frac{x}{a}\right)^2\left(\frac{x}{a}-1\right)^2\left(\frac{12y^2}{b^4}-\frac{12y}{b^3}+\frac{2}{b^2}\right) \tag{2.10a}$$

$$N_{yT}=C\alpha Eha^2\Delta T_1\left(\frac{12x^2}{a^4}-\frac{12x}{a^3}+\frac{2}{a^2}\right)\left(\frac{y}{b}\right)^2\left(\frac{y}{b}-1\right)^2 \tag{2.10b}$$

$$N_{xyT}=-C\alpha Eha^2\Delta T_1\left(\frac{4x^3}{a^4}-\frac{6x^2}{a^3}+\frac{2x}{a^2}\right)\left(\frac{4y^3}{b^4}-\frac{6y^2}{b^3}+\frac{2y}{b^2}\right) \tag{2.10c}$$

2.2.3 Solution of the differential equation

For panels with all edges with simply supported/hinged conditions, the solution of equation (2.2) can be represented as follows:

$$w(x,y,t)=\mathrm{Re}\sum_{m=1}^{\infty}\sum_{n=1}^{\infty}a_{mn}\sin\frac{m\pi x}{a}\sin\frac{n\pi y}{b}e^{i\omega t} \tag{2.11}$$

Here ω is the circular frequency and t is the time. This function satisfies the following kinematic conditions of the panel boundaries,

$$w(0,y,t) = w(a,y,t) = w(x,0,t) = w(x,b,t) = 0 \tag{2.12a}$$

and also the kinetic conditions of the simply supported edges,

$$\frac{\partial^2 w}{\partial x^2}(0,y,t) = \frac{\partial^2 w}{\partial x^2}(a,y,t) = \frac{\partial^2 w}{\partial y^2}(x,0,t) = \frac{\partial^2 w}{\partial y^2}(x,b,t) = 0 \tag{2.12b}$$

After substituting equations (2.3) to (2.6), (2.9) and (2.11) into equation (2.2) and applying the Galerkin's procedure, the following set of equations is obtained for the amplitude coefficients a_{mn}:

$$\left\{\left[r^2 + \left(\frac{a}{b}\right)^2 s^2\right]^2 - R_{xo} r^2 - R_{yo}\left(\frac{a}{b}\right)^2 s^2\right\} a_{rs} - k^2 a_{rs} + \lambda L_{rs} - \frac{4}{\pi^2 D}\frac{a}{b}\left[(I_1)_{rs} + 2\frac{a}{b}(I_2)_{rs} + \left(\frac{a}{b}\right)^2 (I_3)_{rs}\right] = 0 \tag{2.13.a}$$

where

$$k^2 = \frac{\rho_{mat} h a^4 \omega^2}{\pi^4 D}$$

$$R_{xo} = \frac{N_{xo} a^2}{\pi^2 D}$$

$$R_{yo} = \frac{N_{yo} a^2}{\pi^2 D}$$

$$\lambda = \frac{2qa^3}{D\sqrt{M^2 - 1}} \tag{2.14.a,b,c,d.}$$

The parameter k^2 is the non-dimensional frequency. The non-dimensional parameters R_{xo} and R_{yo} accounts for any additional *in-plane* loading along the edges of the panel, either from mechanical sources or from *constraints* to *in-plane thermal expansion* at the edges. The parameter λ is the non-dimensional form of the dynamic pressure. The integral L_{rs} arising due to aerodynamic loading can be expressed as,

$$L_{rs} = \left(\cos\theta (L_1)_{rs} + \frac{a}{b}\sin\theta (L_2)_{rs}\right)$$

$$(L_1)_{rs} = \frac{4}{ab\pi^3}\int_0^b\int_0^a \sum_{m=1}^{\infty}\sum_{n=1}^{\infty} m a_{mn} \cos\frac{m\pi x}{a}\sin\frac{r\pi x}{a}\sin\frac{n\pi y}{b}\sin\frac{s\pi y}{b}\,dxdy$$

$$(L_2)_{rs} = \frac{4}{ab\pi^3}\int_0^b\int_0^a \sum_{m=1}^{\infty}\sum_{n=1}^{\infty} n a_{mn} \sin\frac{m\pi x}{a}\sin\frac{r\pi x}{a}\cos\frac{n\pi y}{b}\sin\frac{s\pi y}{b}\,dxdy \tag{2.15a}$$

The full integral expression of these aerodynamic terms are presented in the Appendix. The integrals $(I_1)_{rs}$, $(I_2)_{rs}$, and $(I_3)_{rs}$ arise due to the non-uniform stress distribution

from the parabolic temperature distribution alone, and they vanish at the edges, or boundaries of the panel. These are given by,

$$(I_1)_{rs} = \int_0^b \int_0^a \sum_{m=1}^{\infty} \sum_{n=1}^{\infty} m^2 a_{mn} \frac{\partial^2 \phi}{\partial y^2} \sin \frac{m\pi x}{a} \sin \frac{r\pi x}{a} \sin \frac{n\pi y}{b} \sin \frac{s\pi y}{b} dxdy \tag{2.15b}$$

$$(I_2)_{rs} = \int_0^b \int_0^a \sum_{m=1}^{\infty} \sum_{n=1}^{\infty} mna_{mn} \frac{\partial^2 \phi}{\partial x \partial y} \cos \frac{m\pi x}{a} \sin \frac{r\pi x}{a} \cos \frac{n\pi y}{b} \sin \frac{s\pi y}{b} dxdy \tag{2.15c}$$

$$(I_3)_{rs} = \int_0^b \int_0^a \sum_{m=1}^{\infty} \sum_{n=1}^{\infty} n^2 a_{mn} \frac{\partial^2 \phi}{\partial x^2} \sin \frac{m\pi x}{a} \sin \frac{r\pi x}{a} \sin \frac{n\pi y}{b} \sin \frac{s\pi y}{b} dxdy \tag{2.15d}$$

$$r = 1,2,3,..... \mathrm{R} \quad s = 1,2,3,..... \mathrm{S}$$

Finally, equation (2.12) can be written as

$$\left\{ \left[r^2 + \left(\frac{a}{b} \right)^2 s^2 \right]^2 - R_{xo} r^2 - R_{yo} \left(\frac{a}{b} \right)^2 s^2 \right\} a_{rs} - k^2 a_{rs} + \lambda L_{rs} + \left\{ \frac{C}{5\pi^2} \left(\frac{a}{b} \right)^2 \left[\left(\frac{r}{s} \right)^2 + \left(\frac{s}{r} \right)^2 \right] a_{rs} + \frac{8C}{\pi^2} \left(\frac{a}{b} \right)^2 K_{rs} \right\} \psi = 0 \tag{2.16}$$

where $$\psi = \frac{\alpha E h a^2 \Delta T_1}{\pi^2 D} \tag{2.17}$$

and

$$K_{rs} = M_{rs} + P_{rs} - 4Q_{rs} - \frac{1}{40} \left[\left(\frac{r}{s} \right)^2 + \left(\frac{s}{r} \right)^2 \right] a_{rs} \tag{2.18}$$

The terms M_{rs}, P_{rs}, Q_{rs} are defined in the Appendix. In order that nontrivial solutions of the system of equation (2.16) exist, it is necessary that the determinant of the coefficients vanish. Thus the stability criterion ultimately reduces to an eigenvalue problem of the following form:

$$\det(A_{ij} - k^2 \delta_{ij}) = 0 \tag{2.19}$$

where k^2 is the eigenvalue, and $\delta_{ij} = \begin{cases} 1 & i = j \\ 0 & i \neq j \end{cases}$ is the kronecker delta.

Since the problem is of determining the stability of a given form of solution, it is advantageous to associate the eigenvalue with the *frequency parameter* k^2. For flow speeds beyond a critical flow velocity V_{cr}, the system becomes *dynamically unstable* when the $\sqrt{-k^2}$ becomes *complex with positive real part.* The imaginary part of $\sqrt{-k^2}$ represents the non-dimensional frequency. This indicates that the system motion diverges in amplitude in an oscillating fashion. Thus from equation (2,19) it is possible to determine the critical values of the non-dimensional dynamic pressure λ_{cr} at which the oscillatory motion of the panel changes from a periodic to an unstable diverging amplitude type. This critical condition is associated with modal coalescence of two or

more modes. For higher ordered modal solutions, the eigenvalues are calculated, and the lowest value of λ_{cr} for which two of the eigenvalues coalesce is sought.

2.3 Effect of Uniform Edge Loading on Flutter Boundary of the panel with flow along *x*-direction.

In-plane edge loading per unit edge length, N_{xo} and N_{yo} on the panel can develop from

(a) Forces from adjacent panels, or movement of the edge supports,
(b) In-plane edge constraints to thermal expansion. Panels with immovable hinged supports can generate such edge loads.

The non-dimensional edge load parameter considered are R_{xo} and R_{yo}, as given by expressions in equations (2.14), are

$$R_{xo} = \frac{N_{xo} a^2}{\pi^2 D} \quad ; \qquad R_{yo} = \frac{N_{yo} a^2}{\pi^2 D} \tag{2.20}$$

The parameter R_{xo} arises from the uniform compressive in-plane load N_{xo} applied on edge *b*, along the *x*- direction while R_{yo} is from the uniform compressive in-plane load N_{yo} on edge *a*, applied perpendicular to the R_{xo} direction. Note that edge loads N_{xo} and N_{yo} are positive for compression, and are given in *N/m* (in SI units). These edge forces, if compressive (positive) in nature, can drastically lead to fall of the critical dynamic pressure of the panel.

Uniform edge loads from in-plane edge constraints to thermal expansion (case (b)), develops due to the difference of *mean* temperature T_{mean} of the panel from the reference temperature $T_{reference}$, at which the edge loading vanishes. One can approximate these edge loads (per unit edge length) from edge constraints to thermal expansion as

$$N_{xo} = N_{yo} = \frac{E}{(1-\mu)} \alpha(\Delta T_2) h \tag{2.21}$$

Thus for this case, $R_{xo} = R_{yo}$. Here the effective panel temperature ΔT_2 for edge loads is defined as

$$\Delta T_2 = T_{mean} - T_{reference} \tag{2.22}$$

The mean panel temperature T_{mean} of the panel with uniform edge temperature T_{edge} and with the parabolic thermal profile *T(x,y)* (as in equation (2.1) is given by

$$T_{mean} = T_{edge} + \frac{\int_{x=0}^{a} \int_{y=0}^{b} T(x,y)\, dy dx}{\int_{x=0}^{a} \int_{y=0}^{b} dy.dx} = T_{edge} + \frac{4}{9} \Delta T_1 \tag{2.23}$$

Thus one can finally express the effective temperature as

$$\Delta T_2 = T_{edge} + \frac{4}{9}\Delta T_1 - T_{reference} \tag{2.24}$$

2.4 Chapter Summary

The analytical formulation for the investigation of supersonic panel flutter under high thermal conditions and arbitrary flow directions is presented here. A parabolic thermal profile over the simply supported panels, without edge constraints is considered. The expressions for the compressive in-plane stress resultants associated with such thermal profiles have been derived and a differential equation of motion of the panel has been presented. It has been shown that the problem reduces to the solution of the eigenvalue problem from which the values of the critical flutter speeds and dynamic pressures can be determined. Critical dynamic pressure is reduced by these compressive in-plane stress resultants from the thermal profiles, even when the edges are free to expand thermally in the plane of the panel.

Edge loading has been shown to arise either from mechanical sources, or from in-plane edge constraints to thermal expansion. Such compressive edge loads also contribute to further reduction in the critical dynamic pressure of the panels.

This formulation will now be used to determine the aeroelastic behavior of the panel with the prescribed thermal profiles, under supersonic flow in arbitrary direction along the plane of the panel. The effects of various flow directions and thermal conditions on the values of the critical (lowest) dynamic pressures for modal coalescence will be investigated.

CHAPTER 3

FLUTTER ANALYSIS WITHOUT THERMAL EFFECTS

3.1 Modal Coalescence in Panel Flutter and Critical Dynamic Pressure

The supersonic panel flutter analysis of rectangular panels simply supported on all edges is considered. The panel is subjected to supersonic airflow in arbitrary direction, but restricted to a plane parallel to the plane of the panel. In this analysis the panel is not subjected to any thermal effects. The values of critical dynamic pressure parameter that lead to flutter for panels of various aspect ratios and different flow direction are determined here. Fig 3.1 presents a schematic view of a hinged panel subjected to supersonic airflow, with flow angle θ with respect to the side *a.*

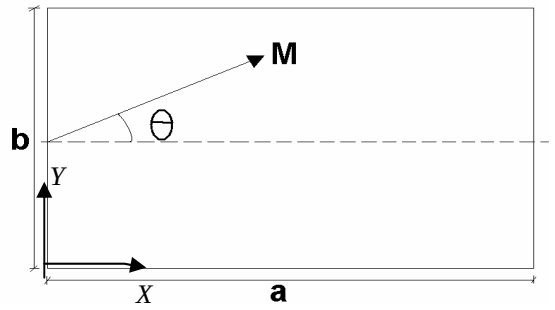

Fig 3.1 Panel under flow along the direction making an angle 'θ' with the edge '*a*' of the panel.

Solution of the characteristic equation (2.13) gives the eigenvalue k^2. In particular, as the non-dimensional dynamic pressure parameter λ increases from zero, two of the free vibration eigenvalues tend to veer towards each other in such a way that for sufficiently large λ (denoted λ_{cr}), they coalesce into a pair of complex–conjugate eigenvalues. One of these complex–conjugate eigenvalues gives a *positive real part* (γ_r >0) for the parameter $\gamma=\gamma_r+j\gamma_i=\sqrt{-k^2}$, indicating dynamic instability, characterized by indefinite divergence of amplitude with respect to time in exponential fashion. Upon such coalescence, one of the corresponding mode amplitude would grow by drawing energy from the flow i.e. the panel would become unstable. The lowest value of λ for which two of the eigenvalues coalesce is the critical value of the dynamic-pressure parameter (λ_{cr}), which leads to flutter.

3.2 Supersonic Panel Flutter analysis for panels of different aspect ratios subjected to airflow along edge *a,* i.e. along *x*-direction

The panel, with hinged end supports, free from temperature effects is considered here. The panel is subjected to a supersonic airflow in *x*-direction. Six normal modes are taken along each of the *x*- and *y*-directions for modal superposition. The critical dynamic

pressure parameter that leads to flutter for an unstressed unheated panel of various aspect ratios is determined. The critical dynamic pressure parameter (λ_{cr}) is determined for different cases. Figures 3.2 and 3.3. show the eigenvalue k^2 variation with λ for aspect ratios of **1** and **2**. It shows the evolution of modes for an increase of dynamic pressure upto λ_{cr}.

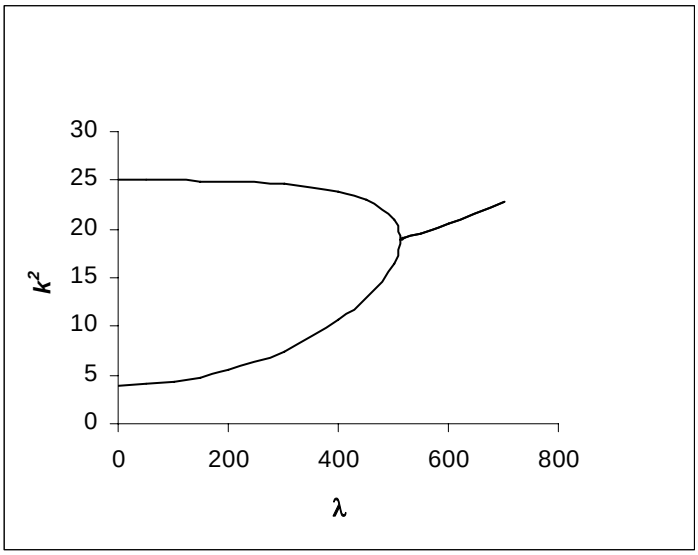

Fig 3.2 Non dimensional Dynamic Pressure λ Vs Non dimensional frequency parameter k^2 for aspect ratio=1

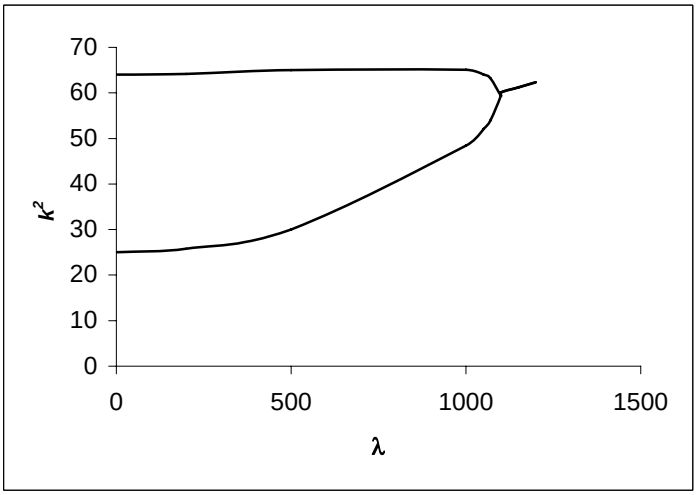

Fig 3.3 Non dimensional Dynamic Pressure λ Vs Non dimensional frequency parameter k^2 for aspect ratio=2

From Fig 3.2 and 3.3, it is observed that for $\lambda = 0$, the eigenvalues are purely real and remain so until some higher value of λ called λ_{cr}, where the two eigenvalues become equal and then form a complex conjugate pair. For the square panel, (*a/b*=1) this instability occurs at $\lambda_{cr} = 512$, from the coalescence of the first two bending modes (*viz* (1,1) and (2,1) modes). For a rectangular panel of aspect ratio *a/b*=2, this instability occurs at $\lambda_{cr} = 1099.9$, from the coalescence of the first two bending modes (*viz* (1,1) and (2,1) modes).

Higher critical dynamic pressures corresponding to coalescence of the higher modes can also be obtained. For the square panel, the higher critical value of the non-dimensional dynamic pressure is 1099.9, which occurs from the coalescence of the third (1,2) mode and the fourth (2,2) mode. Indeed, for the square plate, the third mode (1,2) and the second mode (2,1) are degenerate modes. This is presented in Fig 3.4.

The critical dynamic pressure parameter (λ_{cr}) is determined for different aspect ratios. It is presented in Fig 3.5. Thus for supersonic flow along *x*-direction, the lowest critical dynamic pressure for instability from modal coalescence *increases* with increase of the panel aspect ratio.

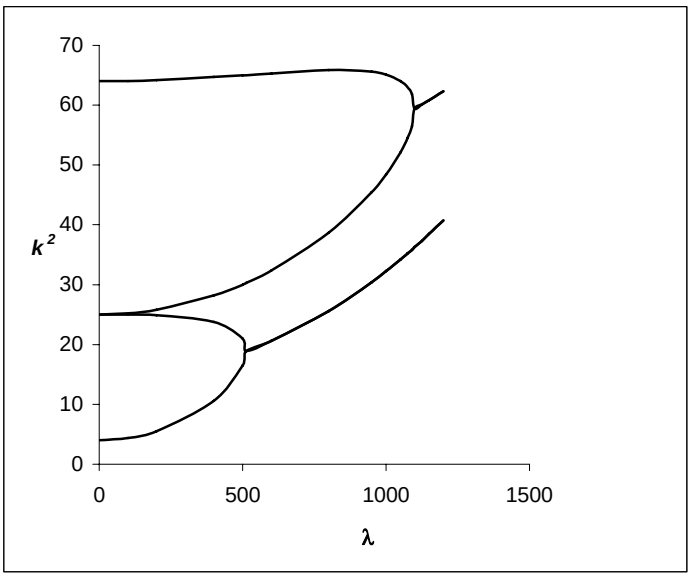

Fig 3.4 Non dimensional Dynamic Pressure λ Vs Non dimensional frequency parameter k^2 for aspect ratio=1 for higher eigenvalues

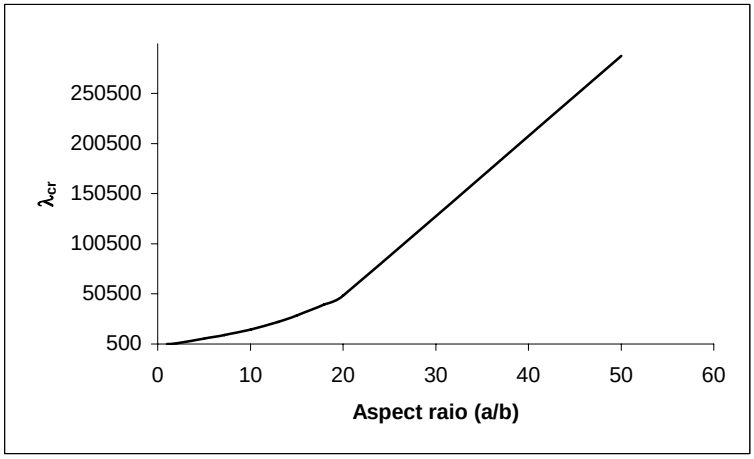

Fig 3.5 Critical Dynamic Pressure Parameter for different Aspect ratios.

3.3 Influence of flow angularity on critical dynamic pressure:

A hinge supported square plate subjected to airflow in arbitrary direction is considered. The flow is along the direction making an angle θ with edge '*a*' of panel. From the analysis using modal superposition as before the critical dynamic pressure value for various flow angels are determined.

For a square plate, a symmetric variation of the critical dynamic pressure is observed, as given is Fig 3.6. The figure shows that for a square panel at $\theta = 0^o$ & $\theta = 90^o$ and $\theta = 30^o$ & $\theta = 60^o$ the values of critical dynamic pressures λ_{cr} are same. The maximum critical dynamic pressure occurs for a flow angle $\theta = 45^o$, *i.e.* for a flow equally inclined to both the edges.

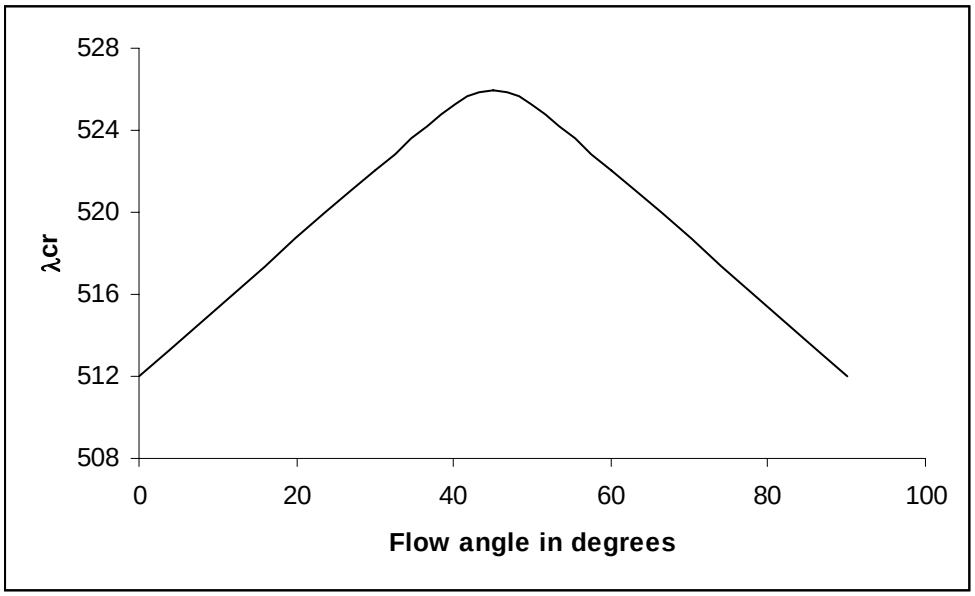

Fig 3.6 Critical dynamic pressure for a square panel with arbitrary flow direction

The results are generated also for panels of aspect ratios 0.5, 2 and 7.2. with different flow angles. Table 3.1 presents the results obtained for rectangular simply supported panels of these aspect ratios subjected to various orientations of the flow. These results are given graphically in Fig 3.7. It is clear that for panels with aspect ratios other than 1, the variation of the dynamic pressure is no more symmetric with the flow angle. For aspect ratios below 1, the critical dynamic pressure λ_{cr} falls with the flow angle, while for aspect ratios above 1, it increases with the flow angle. *This implies that the flow along the longer side is most critical*. *i.e*. the dynamic pressure is lowest for this direction.

Table 3.1. Influence of flow angularity on critical dynamic pressure of panels with different aspect ratios.

a/b	Critical Dynamic Pressure Parameter λ_{cr}				
	$\theta = 0^o$	$\theta = 30^o$	$\theta = 45^o$	$\theta = 60^o$	$\theta = 90^o$
0.5	383.8 *382	215 *213	177 *172	154 *151	138 *135
1	512 *503	522.08 *516	525.95 *523	522.08 *516	512 *503
2	1099.9 *1081	1225 *1206	1409 *1388	1719 *1703	3076.18 *3056
7.2	9387.5	10830	13241	18631	-

*Results obtained by G.Sander, C.Bon and M.Geradin (1973) using finite element analysis [11]

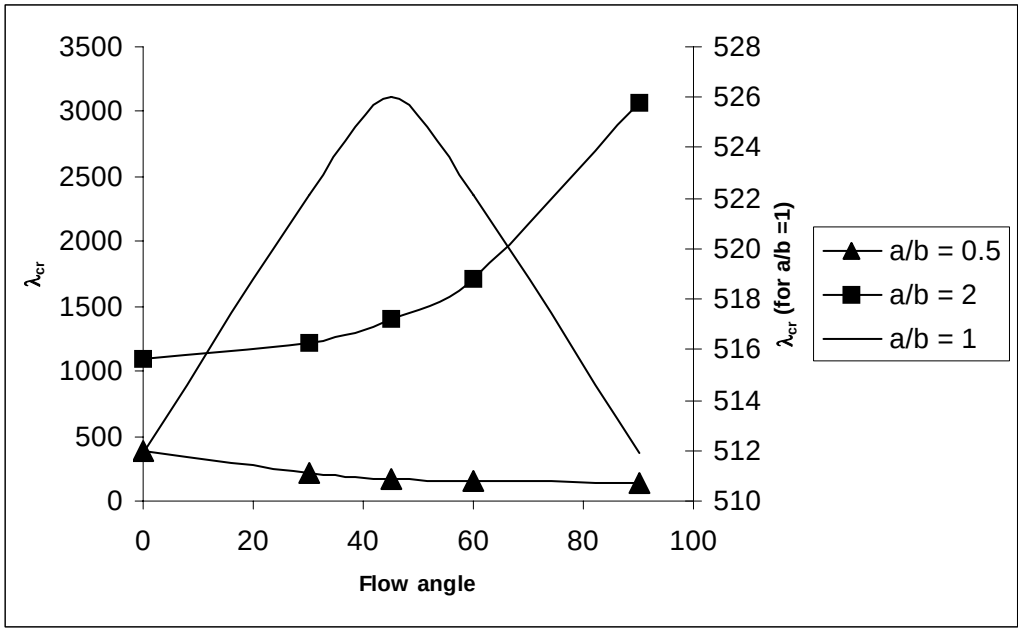

Fig 3.7 Critical dynamic pressure for various aspect ratios with arbitrary flow direction

The value of λ_{cr} is non-dimensionalized with respect to the third power of the edge '*a*' (factor of a^3). Note that the physical dimensional value of the critical dynamic pressure *q* obtained for *a/b*=0.5 and $\theta = 0^o$ is identical to that obtained for *a/b* =2 and $\theta = 90^o$. This is also evident from the corresponding critical values of the non-dimensional dynamic pressures. From Table 3.1, we observe that 383.8 × (2^3)=3076.18. Such a relationship is applicable for all aspect ratios.

3.4 Chapter Summary and Observations

The effect of flow angularity on the critical dynamic pressure for panels of various aspect ratios is studied here.

For supersonic flow along *x*-direction, the lowest critical dynamic pressure for instability from modal coalescence *increases* with increase of the panel aspect ratio.

Investigation of the effect of flow direction reveals that for a square plate the critical dynamic pressure is symmetric with respect to the flow along $\theta = 45^o$**,** at which the maximum critical dynamic pressure occurs.

For other aspect ratios, dynamic pressure decreases as the flow gets more and more aligned to the longest direction. *This implies that the flow along the longer side is most critical*. *i.e*. the critical dynamic pressure is lowest for this direction.

CHAPTER 4

EFFECT OF TEMPERATURE ON FLUTTER BOUNDARY

4.1. Thermal effect on flutter boundary

Thermal stresses are induced in the panel skin due to aerodynamic heating in flight at high speeds. The adverse thermal effect on supersonic flutter boundary due to parabolic temperature distribution and additional compressive edge loads are considered in this analysis. Simply supported rectangular panels of various aspect ratios subjected to supersonic airflow in different direction are treated theoretically.

4.2 Thermal stress distribution due to parabolic temperature distribution

The mid-plane stress resultants N_{xT} , N_{yT} , N_{xyT} due to parabolic temperature distribution (given by equation (2.10) of Chapter 2) are defined by the following equation:

$$N_{xT} = C\alpha Eha^2 \Delta T_1 \left(\frac{x}{a}\right)^2 \left(\frac{x}{a}-1\right)^2 \left(\frac{12y^2}{b^4} - \frac{12y}{b^3} + \frac{2}{b^2}\right) \tag{4.1}$$

$$N_{yT} = C\alpha Eha^2 \Delta T_1 \left(\frac{12x^2}{a^4} - \frac{12x}{a^3} + \frac{2}{a^2}\right)\left(\frac{y}{b}\right)^2 \left(\frac{y}{b}-1\right)^2 \tag{4.2}$$

$$N_{xyT} = -C\alpha Eha^2 \Delta T_1 \left(\frac{4x^3}{a^4} - \frac{6x^2}{a^3} + \frac{2x}{a^2}\right)\left(\frac{4y^3}{b^4} - \frac{6y^2}{b^3} + \frac{2y}{b^2}\right) \tag{4.3}$$

The variation of stress resultants N_{xT} and N_{yT} due to parabolic temperature distribution over the panel of aspect ratio (a/b =1) is shown in Figs 4.1.a. & 4.1.b. The variation of stress resultant N_{xyT} due to temperature distribution over the panel of aspect ratio a/b =1 is shown in Fig 4.1.c. Note that these stress resultants vanish at the panel boundaries.

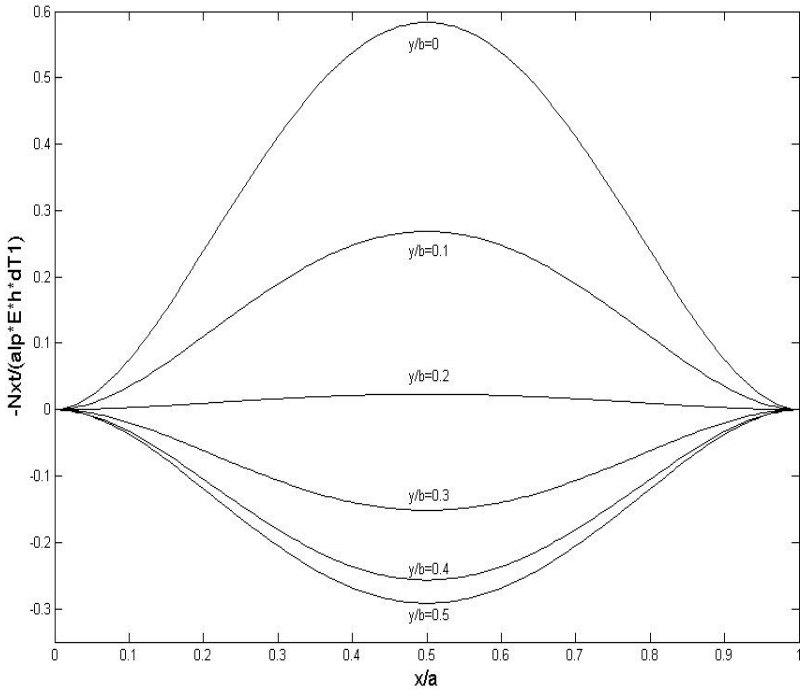

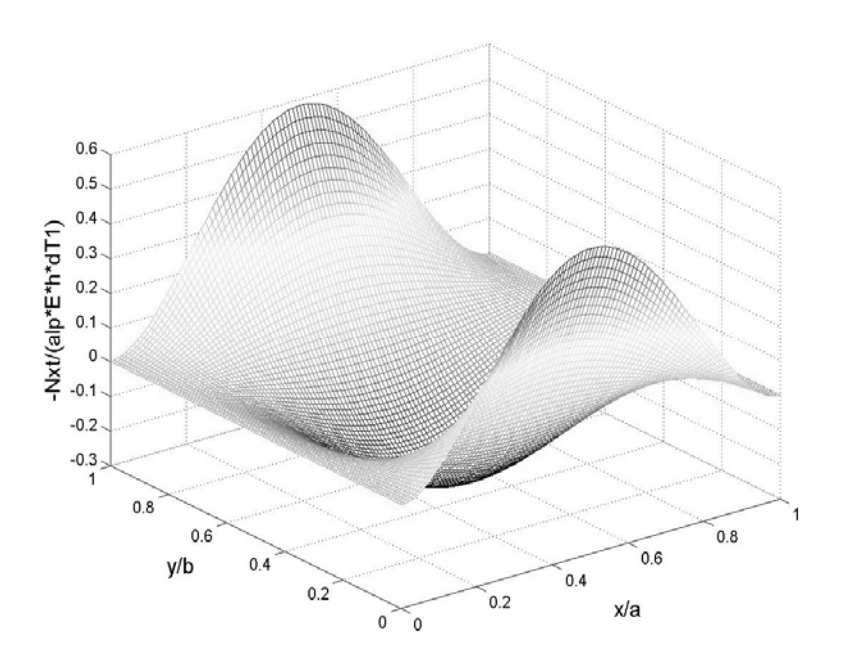

Fig 4.1.a Normal stress resultant N_{xT} for a square panel subjected to parabolic temperature distribution.

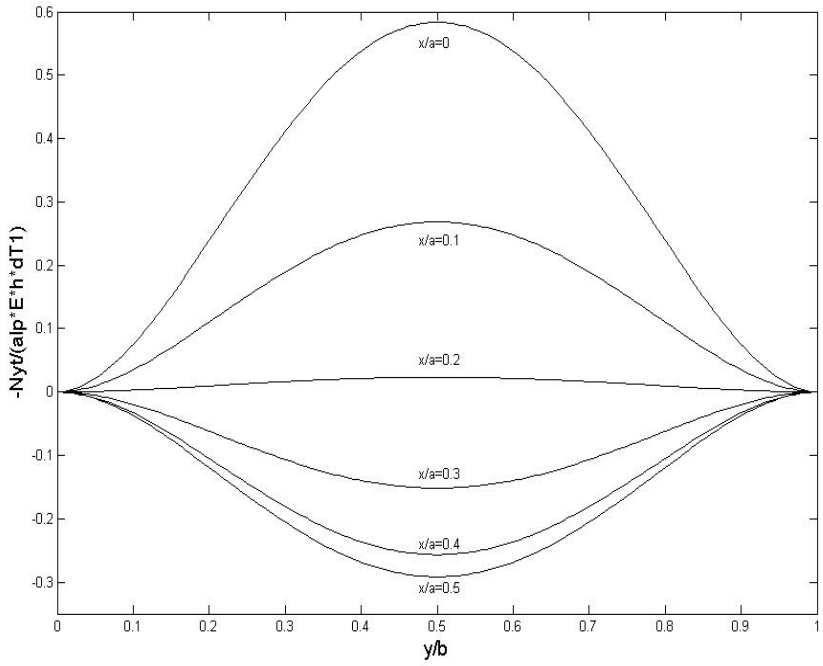

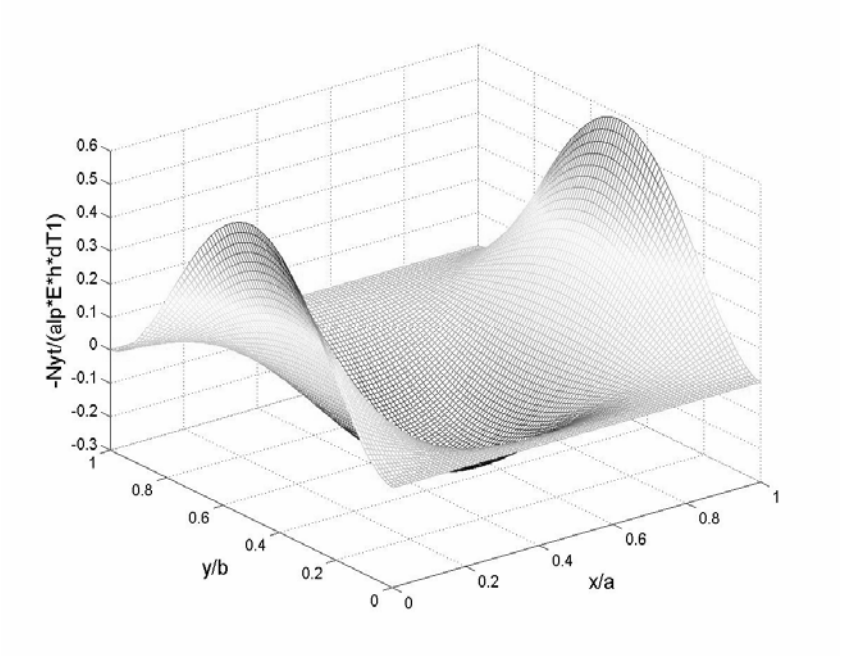

Fig 4.1.b Normal stress resultant N_{yT} for a square panel subjected to parabolic temperature distribution.

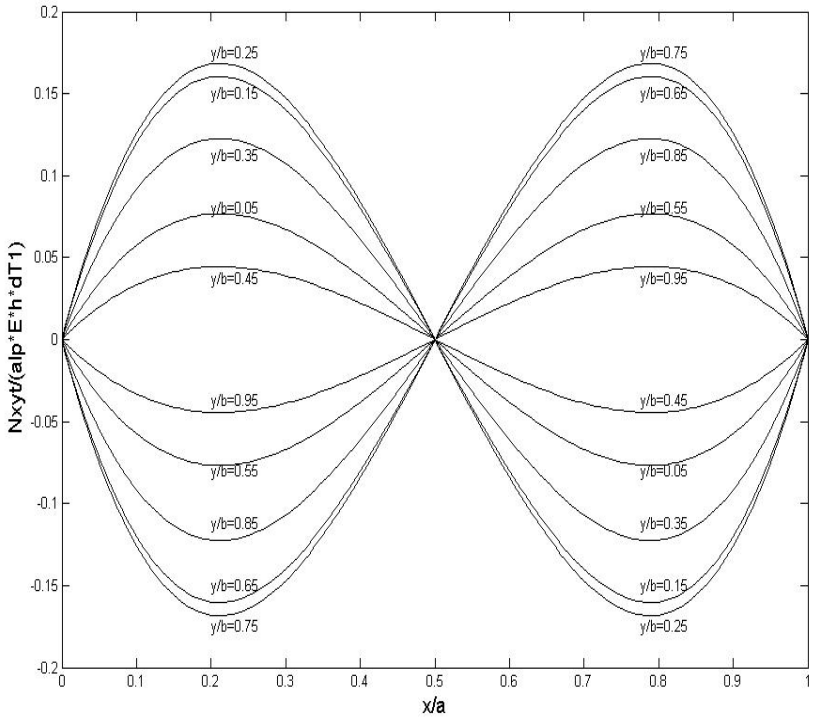

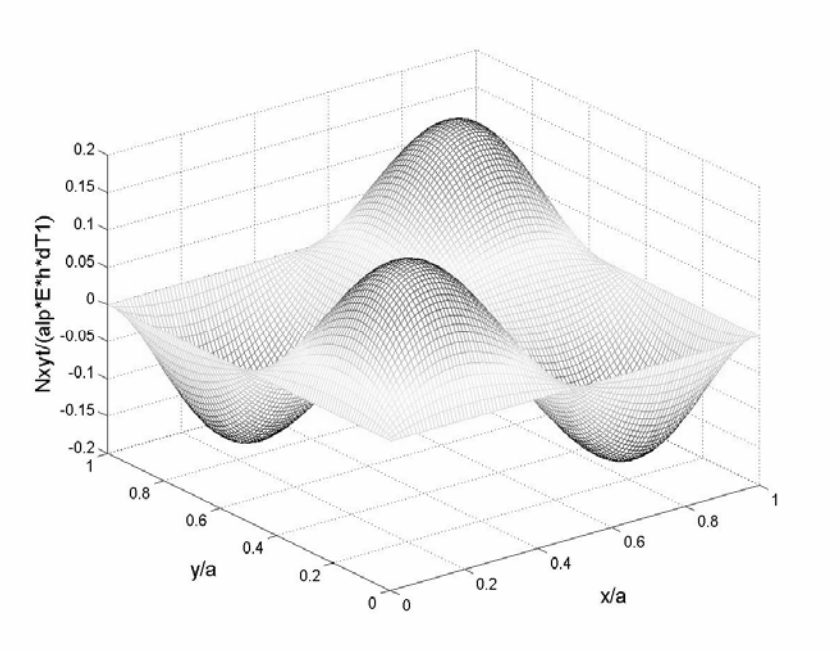

Fig 4.1.c Shear stress resultant N_{xyT} for a square panel subjected to parabolic temperature distribution

4.3. Effect of Parabolic Temperature Distribution on Flutter Boundary for a square panel subject to airflow along *x*-direction (edge *a*)

Fig 4.2 shows the effect of the parabolic temperature distribution on the flutter behavior of a square panel free of uniform mid-plane stresses. The results of the analysis are generated with superposition of 6 modes along flow (x-direction) and 3 modes along the cross-flow direction (y-direction) are considered for getting the converging solution. *i.e. R=6*; *S=3*. (Refer to the Equation 2.14 and Chapter2 / Article 2.2.3). From Fig 4.2, it can be observed that there is a significant fall in the critical dynamic pressure with rise in temperature value at the panel center.

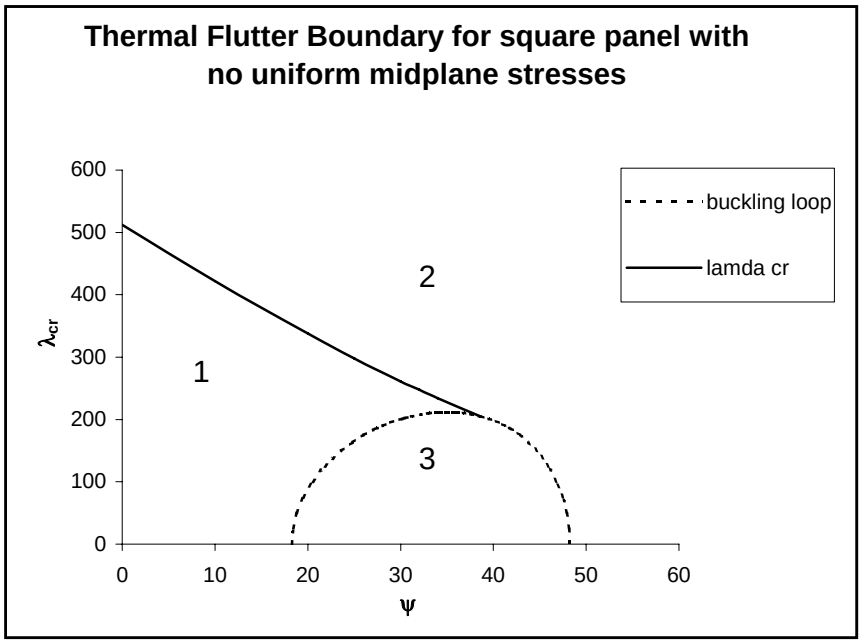

Fig 4.2 Variation of Critical Dynamic Pressure Parameter for flow direction along edge *a*, i.e. x axis, with parabolic temperature distribution amplitude parameter ($\psi = \frac{\alpha E h a^2 \Delta T_1}{\pi^2 D}$) over the square plate.

The three regions shown in Fig 4.2 are characterized by the value of frequency parameter squared (k^2).

Region	k^2	ω
1	Real & positive	Real
2	Complex	Complex (one root lead to oscillating, divergent panel motion)
3	Negative	Pure imaginary

In region 1, the panel is flat and there is no flutter. i.e. the panel oscillation is stable. In the region 2, the panel is dynamically unstable. In the region 3, the panel is buckled. i.e. the panel is statically unstable. In this region, the panel undergoes indefinite

exponential increase of displacements, till structural failure, without any oscillatory motion (divergence).

These three regions are separated by two boundaries. The first is the buckling loop, which is the locus of points for which $k^2 = 0$. The second is the flutter boundary, which is the locus of points at which two frequencies coalesce. The point of tangency of the flutter boundary with the buckling loop represents the lowest value of λ_{cr} associated with this panel configuration.

4.4. Effect of Parabolic Temperature Distribution on Flutter Boundary for a square panel with arbitrary flow direction

The flutter boundary of a square simply supported panel subjected to airflow in arbitrary direction is determined. The effect of parabolic temperature distribution over the panel is considered. Fig 4.3 shows the effect of parabolic temperature distribution over a panel of aspect ratio =1 (square panel), when the panel is subjected to airflow in arbitrary direction. The results of the analysis are generated with superposition of 6 modes along x-direction and 6 modes along the y-direction *i.e. R=6; S=6.* For arbitrary flow direction it is required to take same number of modes along both x and y direction to get the convergent solution. For a square panel at $\theta = 0^o$ and $\theta = 90^o$ the value of critical dynamic pressure λ_{cr} is same. It is also same at $\theta = 30^o$ and $\theta = 60^o$. This is evident from symmetry conditions in the square panel. The variation of critical dynamic pressure parameter for a square panel with different temperature distribution amplitude parameter for various flow angle is presented in Table 4.1.

Table 4.1. **Critical dynamic pressure of a square panel for various temperature distribution amplitude parameter (ψ) and flow angle.**

	Critical Dynamic Pressure parameter λ_{cr}				
	$\theta = 0^o$	$\theta = 30^o$	$\theta = 45^0$	$\theta = 60^o$	$\theta = 90^o$
$\psi = 0$	512	522.1	526	522.1	512
$\psi = 10$	421.9	429.4	432.2	429.4	421.9
$\psi = 20$	337.5	342.6	344.4	342.6	337.5
$\psi = 30$	261.2	264.3	265.4	264.3	261.2

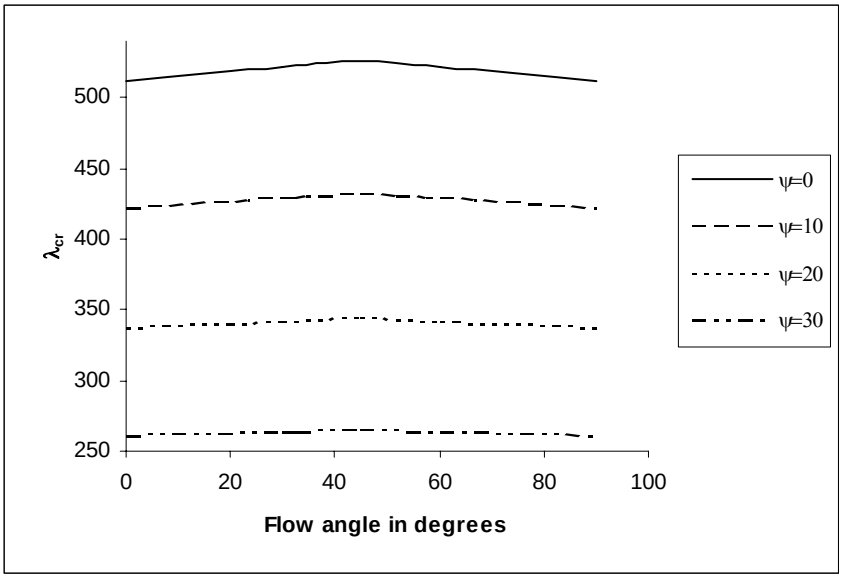

Fig 4.3 Critical dynamic pressure variation with flow angle for different parabolic temperature profiles ($\psi = \frac{\alpha E h a^2 \Delta T_1}{\pi^2 D}$) over a square panel.

4.5 Effect of Panel Aspect Ratio on Flutter Boundary with Parabolic Temperature Profile and air flow along x-direction

Critical dynamic pressure parameter values for supersonic flow along side *a* of flat rectangular panels of various aspect ratios and thermal conditions are computed.

Flutter boundary variation with parabolic thermal profile parameter ψ for a rectangular panel of aspect ratio=*2* for flow along the *x*-direction (side *a*) is presented in Fig 4.4.

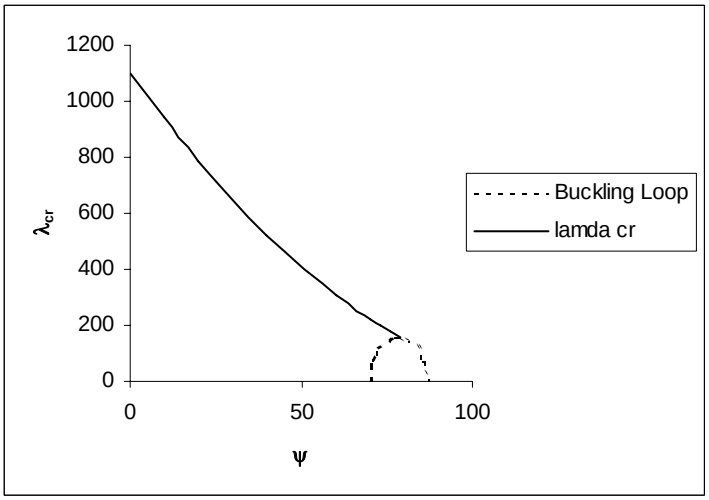

Fig 4.4 Variation of Critical Dynamic Pressure Parameter with parabolic temperature profile over the panel of aspect ratio=2 subjected to supersonic flow along x-direction.

Variation of flutter boundary with the thermal profile for three chosen panel aspect ratios is shown in Fig 4.5. The various curves drawn are for aspect ratios of **0.5**, **1** and **2**. For all cases, the flutter boundary (critical dynamic pressure) falls steeply with rise in temperature at the panel center.

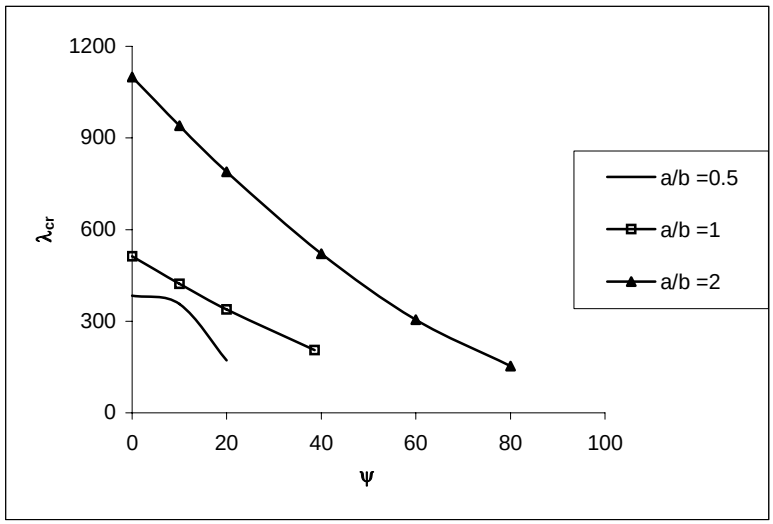

Fig 4.5 Variation of Critical Dynamic Pressure Parameter due to parabolic temperature distribution over the panel for different aspect ratios.

A particular case of aspect ratio = 7.2 (a typical case of wing panels used in re-entry vehicles) is considered and the variation of critical dynamic pressure parameter due to the parabolic temperature distribution is presented in Fig 4.6.

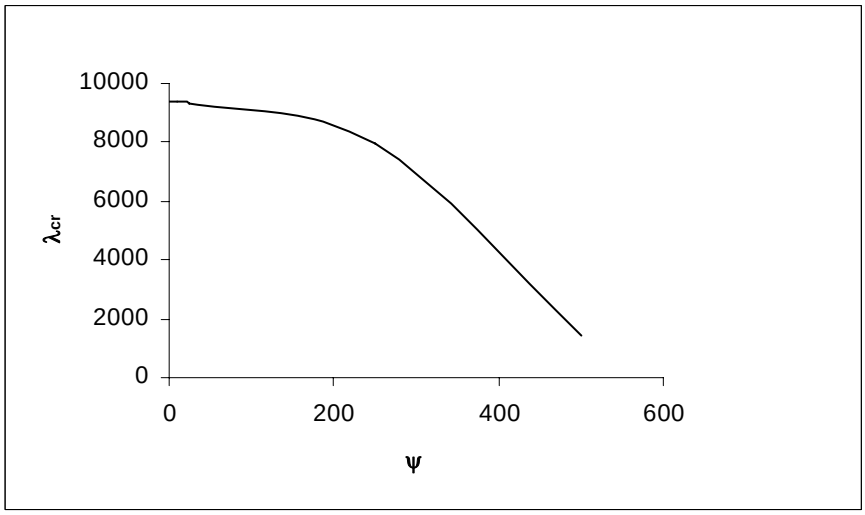

Fig 4.6 Variation of Critical Dynamic Pressure Parameter due to parabolic temperature distribution over the panel of aspect ratio=7.2 and the flow is along x-direction.

4.6 Effect of Flow Direction on Flutter Boundary for panels of various aspect ratios with Parabolic Temperature Distribution

The effect of flow direction on the flutter boundary parameter λ_{cr} of rectangular simply supported panels under the effect of parabolic temperature distribution profile is investigated. The flow is considered to be parallel to the panel plane, and inclined at an angle of θ with the edge *a* (*x*-axis), (see Fig 2.1). The results are generated for panels of different aspect ratios. The variation of critical dynamic pressure parameter values for a panels of aspect ratios = 0.5, 2 and 7.2 with different temperature distribution amplitude parameter and flow angles are presented in Table 4.2-4.4.

The graphical representation of the variation of the critical dynamic pressure parameter values for these aspect ratios with flow angle and parabolic thermal file profile are presented in Figures 4.7-4.9. For all these cases, it can again be observed that for a given temperature profile, the critical dynamic pressure falls as the flow tends towards the longer direction of the panel. Also, for a given flow direction and given aspect ratio, the value of critical dynamic pressure falls with temperature. Thus one can conclude that both thermal conditions and flow direction affect the flutter boundary.

Table 4.2 Critical dynamic pressure of a panel of aspect ratio *a/b*= 0.5 for various temperature distribution amplitude parameter (ψ) and flow angle θ.

	Critical Dynamic Pressure parameter λ_{cr}				
	$\theta = 0^o$	$\theta = 30^o$	$\theta = 45^0$	$\theta = 60^o$	$\theta = 90^o$
$\psi = 0$	383.8	214.9	176.1	153.2	137.5
$\psi = 10$	355.7	116.4	88.4	74.1	65.1
$\psi = 20$	171.3	37.4	26.9	22.1	19.2

Table 4.3 Critical dynamic pressure of a panel of aspect ratio *a/b* = 2 for various temperature distribution amplitude parameter (ψ) and flow angle θ.

	Critical Dynamic Pressure parameter λ_{cr}				
	$\theta = 0^o$	$\theta = 30^o$	$\theta = 45^0$	$\theta = 60^o$	$\theta = 90^o$
$\psi = 0$	1099.9	1225	1408.2	1718.9	3070.4
$\psi = 10$	939.4	1053	1222.5	1521.5	3015
$\psi = 20$	788.5	889	1042.1	1322.4	2959.1
$\psi = 30$	648.5	734.9	869.2	1124.6	2774

Table 4.4 Critical dynamic pressure of a panel of aspect ratio *a/b*=7. 2 for various temperature distribution amplitude parameter (ψ) and flow angle θ.

	Critical Dynamic Pressure parameter λ_{cr}			
	$\theta = 0^o$	$\theta = 30^o$	$\theta = 45^0$	$\theta = 60^o$
$\psi = 0$	9387.5	10830	13241	18631
$\psi = 100$	9298	10727	13116	18457
$\psi = 250$	7940	9137	11121	15447
$\psi = 400$	3550	4095	5003	7025

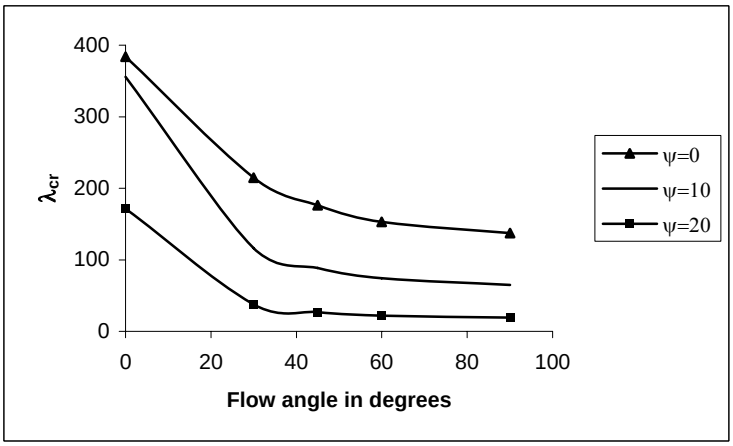

Fig 4.7 Critical dynamic pressure for various flow angles with parabolic temperature distribution over panel of aspect ratio *a/b*=0.5.

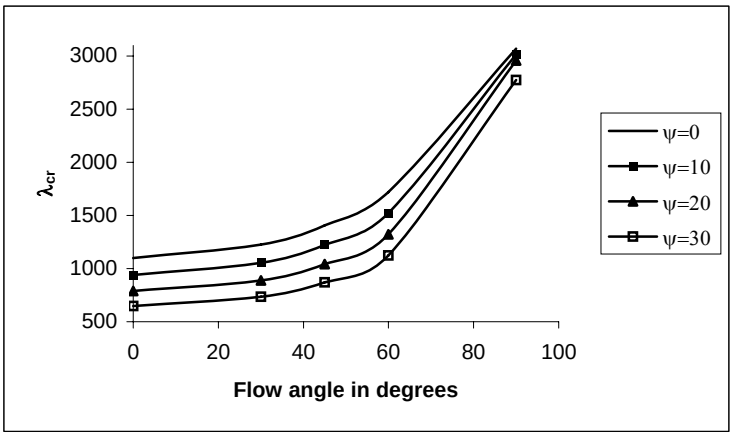

Fig 4.8 Critical dynamic pressure for various flow angles with parabolic temperature distribution over panel of aspect ratio *a/b*=2.

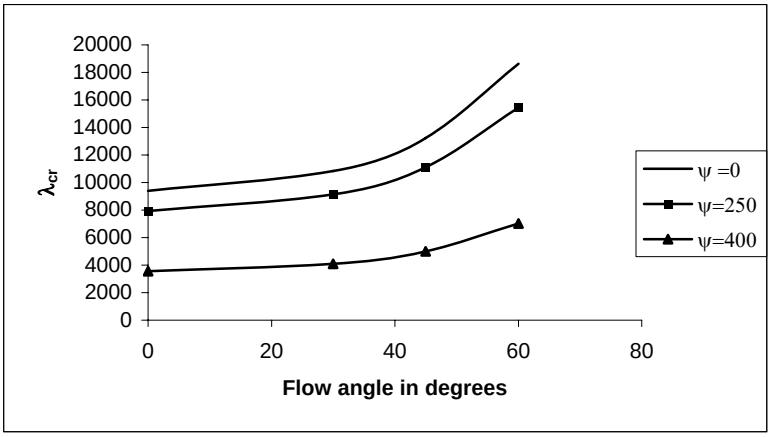

Fig 4.9 Critical dynamic pressure for various flow angle with parabolic temperature distribution over panel of aspect ratio = 7.2.

4.7 Effect of Uniform Edge Loading on Flutter Boundary of the panel with flow along *x*-direction (edge *a*)

In-plane edge loading per unit edge length, N_{xo} and N_{yo} on the panel can develop from

(a) Forces from adjacent panels, or movement of the edge supports,
(b) In-plane edge constraints to thermal expansion. Panels with immovable hinged supports can generate such edge loads.

The non-dimensional edge load parameter considered are R_{xo} and R_{yo}, as given by expressions in equations (2.20) of Chapter 2.

$$R_{xo} = \frac{N_{xo} a^2}{\pi^2 D} \quad ; \qquad R_{yo} = \frac{N_{yo} a^2}{\pi^2 D} \tag{4.4a,b}$$

These edge forces, if compressive (positive) in nature, can drastically lead to fall of the critical dynamic pressure of the panel.

Thus along with the thermally induced loading N_{xT}, N_{yT} and N_{xyT} due to the parabolic thermal profile with no in-plane edge constraints at the simply supported edges, the edge forces bring about further fall of the dynamic pressure. The variation of flutter boundary of a square panel subjected to airflow along edge *a* (along *x*-direction) due to the effect of both the uniform edge loading R_{xo} and R_{yo} (with $R_{xo} = R_{yo}$) and a parabolic temperature profile is investigated. The results for aspect ratios 1,2 and 7.2 are presented in Table 4.5-4.7. It must be noted that these results are generated by taking the *net* edge loads (N_x, N_y, N_{xy}) as given in equation (2.4), i.e. the contributions of the in-plane stress resultants (N_{xT}, N_{yT}, N_{xyT}) from the parabolic profile are superposed with those from the edge loads (N_{x0}, N_{y0}).

For edge loads from in-plane edge constraints to thermal expansion (case (b)), the uniform edge loading develops due to the difference of *mean* temperature T_{mean} of the panel from the reference temperature $T_{reference}$, at which the edge loading vanishes. One can approximate these edge loads (per unit edge length) from edge constraints to thermal expansion as

$$N_{xo} = N_{yo} = \frac{E}{(1-\mu)} \alpha (\Delta T_2) h \tag{4.5}$$

Thus for this case, $R_{xo} = R_{yo}$. Here the effective panel temperature ΔT_2 for edge loads is defined as in equations (2.22) and (2.24),

$$\Delta T_2 = T_{mean} - T_{reference} = T_{edge} + \frac{4}{9} \Delta T_1 - T_{reference} \tag{4.6}$$

The effects of edge loading from in-plane edge constraints on thermal expansion upon the critical dynamic pressure is demonstrated for two specimens of aluminium panels of aspect ratios 1 and 7.2.

Table 4.5 Critical dynamic pressure values of a panel of aspect ratio *a/b* = 1 for various edge load parameter ($R_{xo} = R_{yo}$) and parabolic temperature distribution amplitude parameter (ψ) with flow along edge *a* (*x*-direction). Positive Edge loads signify compression.

	Critical Dynamic Pressure parameter λ_{cr}			
	$R_{xo} = -3$	$R_{xo} = -1$	$R_{xo} = 0$	$R_{xo} = 2$
$\psi = 0$	792.18	602.01	512	343.2
$\psi = 10$	684.75	505.8	421.95	266.6
$\psi = 20$	580.9	414.4	337.45	197.5
$\psi = 30$	481.33	329.65	261.05	Divergence

Table 4.6 Critical dynamic pressure values of a panel of aspect ratio *a/b* = 2 for various edge load parameter ($R_{xo} = R_{yo}$) and parabolic temperature distribution amplitude parameter (ψ) with flow along edge *a* (*x*-direction). Positive Edge loads signify compression.

	Critical Dynamic Pressure parameter λ_{cr}			
	$R_{xo} = -3$	$R_{xo} = 0$	$R_{xo} = 2$	$R_{xo} = 4$
$\psi = 0$	1430	1099.9	892	696
$\psi = 10$	1254	939.4	745	563
$\psi = 20$	1084	788.5	608	442
$\psi = 30$	924	648.5	484	335

Table 4.7 Critical dynamic pressure values of a panel of aspect ratio *a/b* =7.2 for various edge load parameter ($R_{xo} = R_{yo}$) and parabolic temperature distribution amplitude parameter (ψ) with flow along edge *a* (*x*-direction). Positive Edge loads signify compression.

	Critical Dynamic Pressure parameter λ_{cr}			
	$R_{xo} = -3$	$R_{xo} = 0$	$R_{xo} = 50$	$R_{xo} = 80$
$\psi = 0$	9555	9387.5	6402	2948
$\psi = 100$	9466	9300	4709	1053

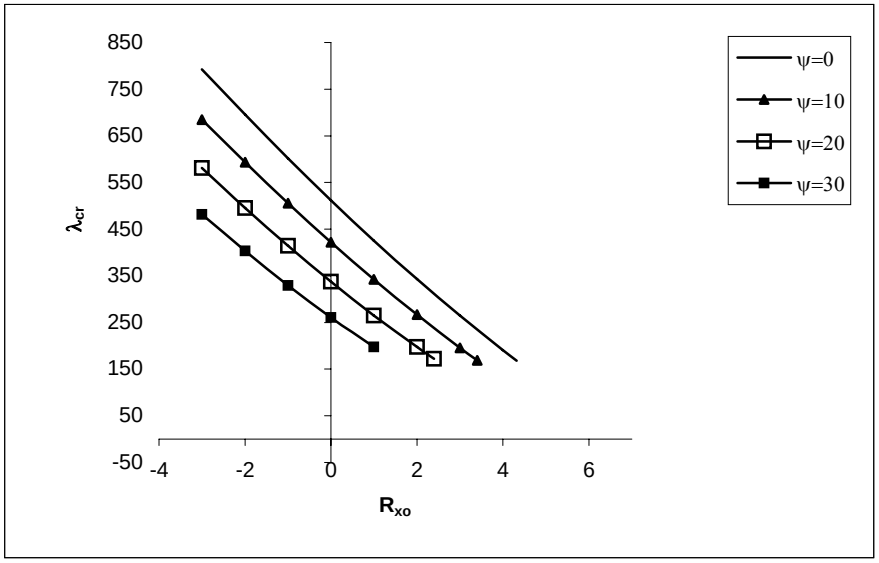

Fig 4.10 Effect of Uniform Edge Loading on Flutter Boundary and Parabolic Temperature profile on critical dynamic pressure for a square panel. Flow along x-direction.

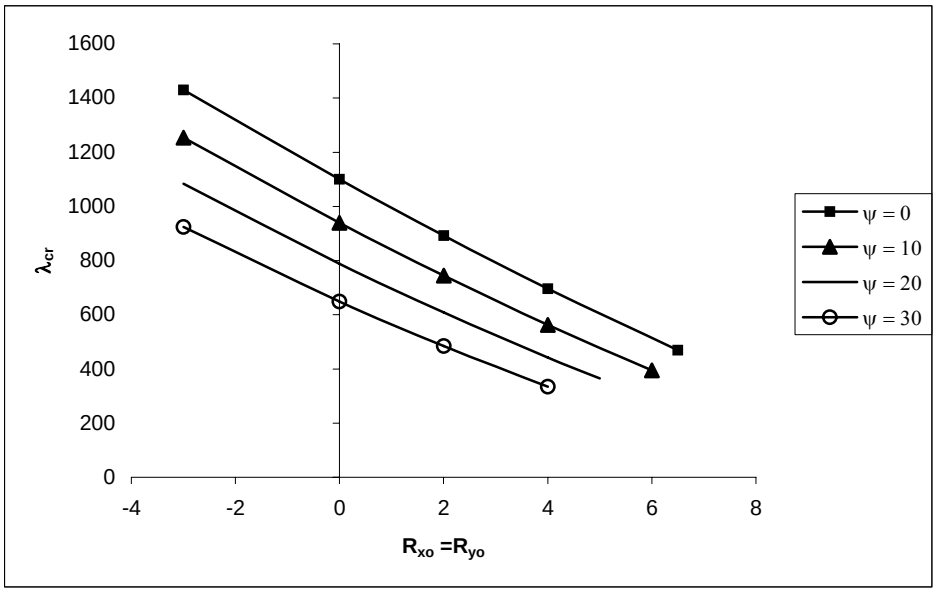

Fig 4.11 Effect of Uniform Edge Loading on Flutter Boundary and Parabolic Temperature profile on critical dynamic pressure for a panel of aspect ratio *a/b*=2. Flow along x-direction.

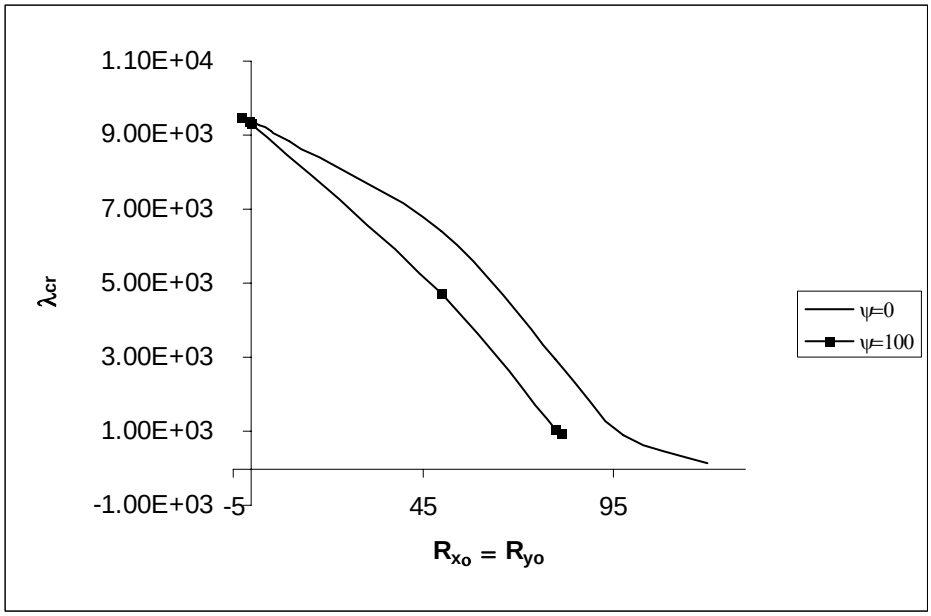

Fig 4.12 Effect of Uniform Edge Loading on Flutter Boundary and Parabolic Temperature profile on critical dynamic pressure for a panel of aspect ratio *a/b*=7.2. Flow along x-direction.

4.8 Effect of Flow Direction on Flutter Boundary for panels of various aspect ratios with Edge Loading and Parabolic Temperature Distribution

The variation of flutter boundary of panels of various aspect ratios **1,2 &7.2** subjected to airflow in arbitrary direction, due to the effect of both the uniform edge loading and parabolic temperature distributions is investigated. The results are presented in Figures 4.13-4.15.

The critical dynamic pressure value is always more than what it would have been if the flow is along the longer edge. Thus for design purposes, the least value of the critical dynamic pressure, that occurs only for flow along the longer edge, is to be considered.

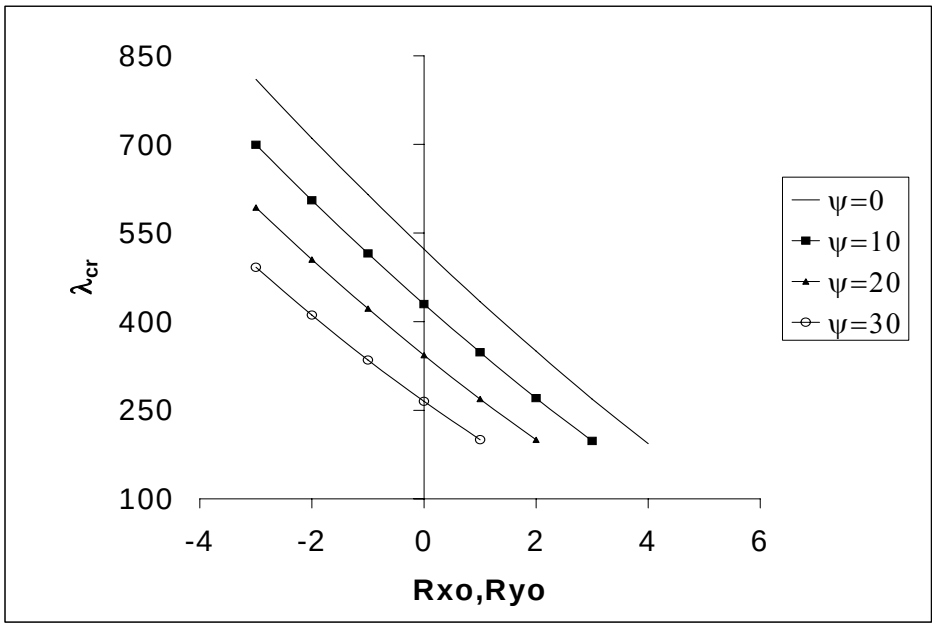

(a)

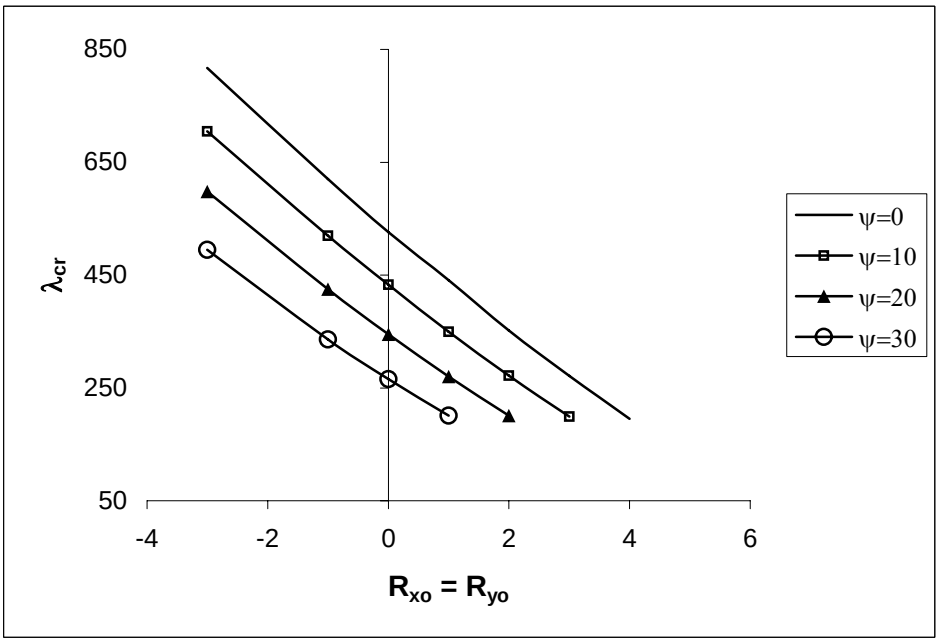

(b)

Fig 4.13 Effect of Edge loading and Parabolic Thermal Profile on Flutter boundary of a square panel with flow angle of a) $\theta = 30^0$ **& b)** $\theta = 45^0$

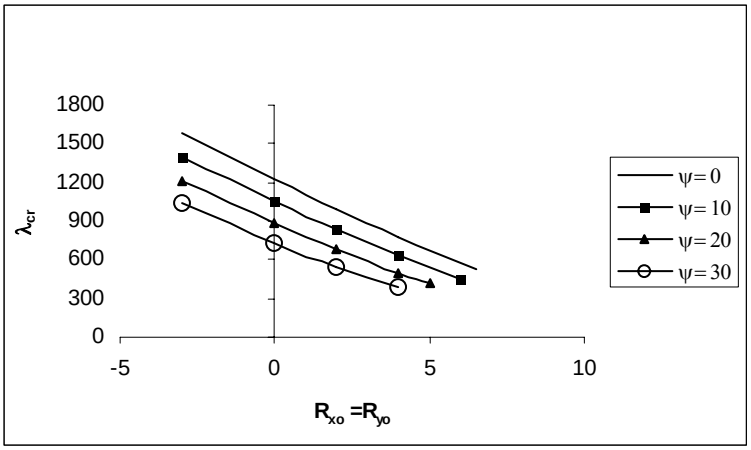

(a)

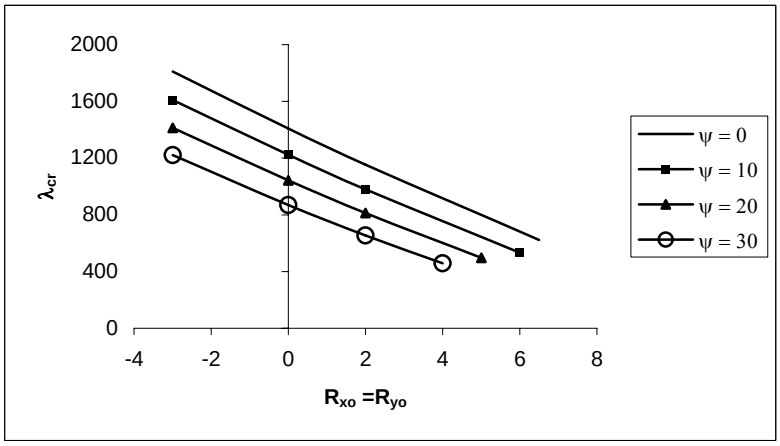

(b)

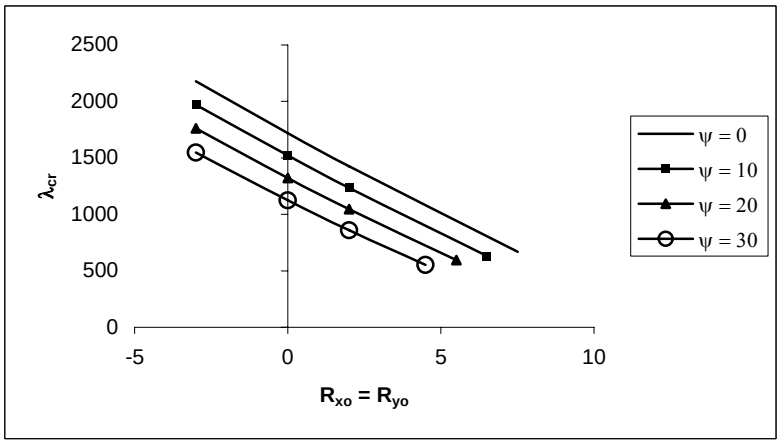

(c)

Fig 4.14 Effect of Edge loading and Parabolic Thermal Profile on Flutter boundary of a panel of aspect ratio *a/b*=2with flow angle of a) $\theta = 30^0$ **& b)** $\theta = 45^0$ **c)** $\theta = 60^0$

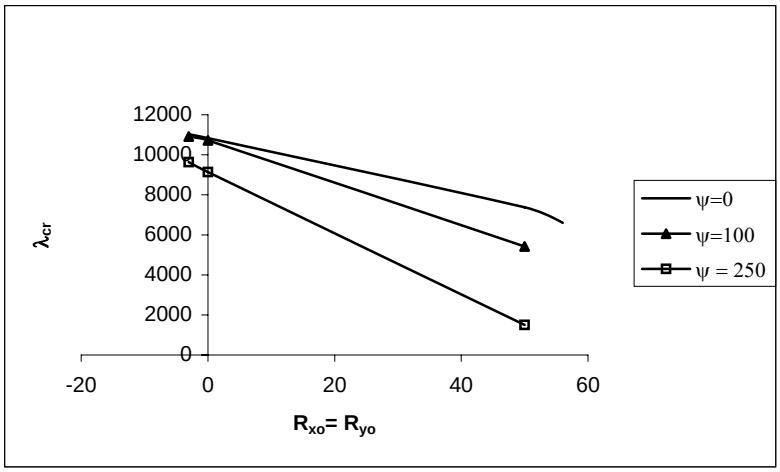

(a)

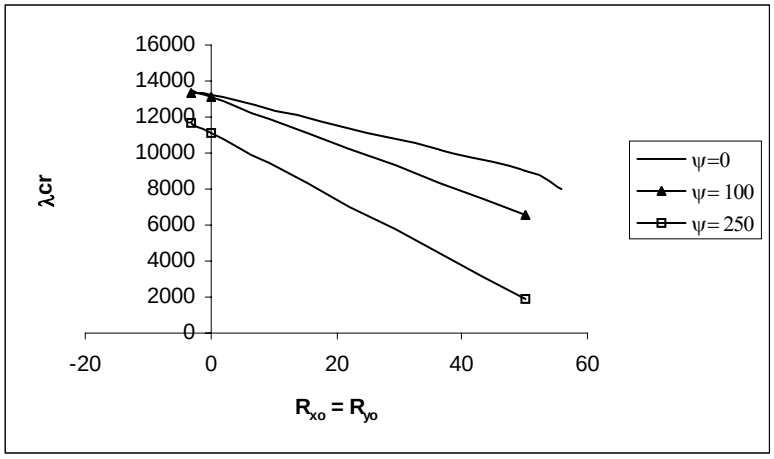

(b)

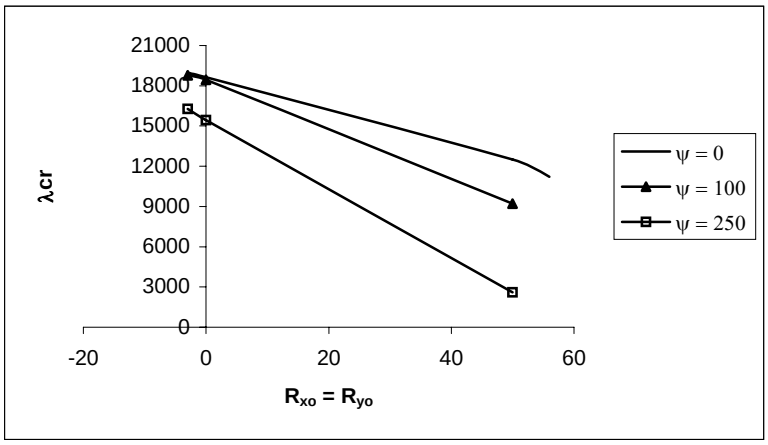

(c)

Fig 4.15 Effect of Edge loading and Parabolic Thermal Profile on Flutter boundary of a panel of aspect ratio *a/b*=7.2with flow angle of a) $\theta = 30^0$ **& b)** $\theta = 45^0$ **c)** $\theta = 60^0$

4.9 Chapter Summary and Observations

The adverse thermal effect on supersonic flutter boundary of panels with different aspect ratios subjected to flow in arbitrary direction due to parabolic temperature distribution over the panel and due to edge loads is investigated. These edge loads can arise from in-plane edge constraints to thermal expansion due to the difference of ambient temperature from the reference temperature. Panels with hinged supports at all edges can develop such in-plane loadings.

The critical dynamic pressure λ_{cr} decreases as the parabolic temperature distribution amplitude parameter increases. It can be observed that there is a significant fall in the critical dynamic pressure with rise in temperature value at the panel center. For all cases of different aspect ratios, the flutter boundary (critical dynamic pressure) falls steeply with rise in temperature at the panel center. Also the critical dynamic pressure parameter λ_{cr} decreases as the edge load parameter increases.

It can be observed that for a given temperature profile the critical dynamic pressure falls as the flow tends towards the longer direction of the panel. Also, for a given flow direction and given aspect ratio, the value of critical dynamic pressure falls with temperature. Thus one can conclude that both thermal conditions and flow direction affect the flutter boundary. Compressive edge loads cause further reduction of the critical dynamic pressure.

CHAPTER 5

NUMERICAL RESULTS FOR PANELS OF GIVEN CONFIGURATION

5.1. Numerical Studies for Supersonic Panel Flutter

A numerical study of the supersonic flutter boundary of panels of given dimensions and material properties is made and the results are presented here. Aluminium panels of aspect ratios of 1 and 7.2 are studied. The variation of critical parameters (flutter dynamic pressure/ flutter velocity) with parabolic temperature distribution over the panel is investigated for different flow directions. The effects of edge loads that arise from in-plane constraints are also simulated. The results for no thermal condition are validated with finite element software, NASTRAN.

5.2. Numerical Results for a square panel of aluminium (Specimen A) using theoretical formulation

Consider a simply supported square panel subjected to supersonic airflow over one surface with the following dimensions and properties.

Length of panel, a = $0.25m$
Width of panel, b = $0.25m$
Aspect ratio, a/b = 1
Thickness of panel, h = $0.00232m$
Modulus of Elasticity, E = $70\text{x}10^{9}\ N/m^{2}$
Poisson's ratio, μ = 0.3
Coefficient of thermal expansion of Aluminium
α = $2.3\text{x}10^{-5}/^{o}C$
Density of material, ρ_{mat} = $2764\ kg/m^{3}$

Density of air, ρ_{air} = $1.225\ kg/m^{3}$

Bending rigidity, D = $\dfrac{Eh^{3}}{12\left(1-\mu^{2}\right)}$ = 80.046 Nm

Dynamic pressure, q = $\dfrac{1}{2}\rho_{air}V^{2}$ (V=Flow speed)

Mach number, M = $\dfrac{V}{V_{sound}}$

Velocity of sound, V_{sound} = $340m/s$

Dynamic pressure parameter

$$\lambda \quad = \quad \frac{2qa^3}{D\sqrt{M^2-1}} = \frac{0.000239v^2}{\sqrt{\left(\frac{v}{340}\right)^2-1}}$$

5.2.1 Effect of Parabolic Temperature Distribution over the panel when airflow along x-direction (edge a)

For the given panel (specimen A) on simply supported edges, the critical velocity values are calculated for various values of parabolic profile parameter ΔT_1. The non-dimensional temperature parameter is used for computing the physical temperature amplitude ΔT_1 (in degrees centigrade) for the parabolic profile for the specimen panel A of Article 5.2.

$$\psi \quad = \quad \frac{\alpha E h a^2 \Delta T_1}{\pi^2 D} \quad = \quad 0.2958\Delta T_1 .$$

The variations of critical parameters (critical dynamic pressure, critical velocity, critical Mach number) due to the parabolic temperature distribution over the given panel of aspect ratio=1 are shown in Fig 5.1.

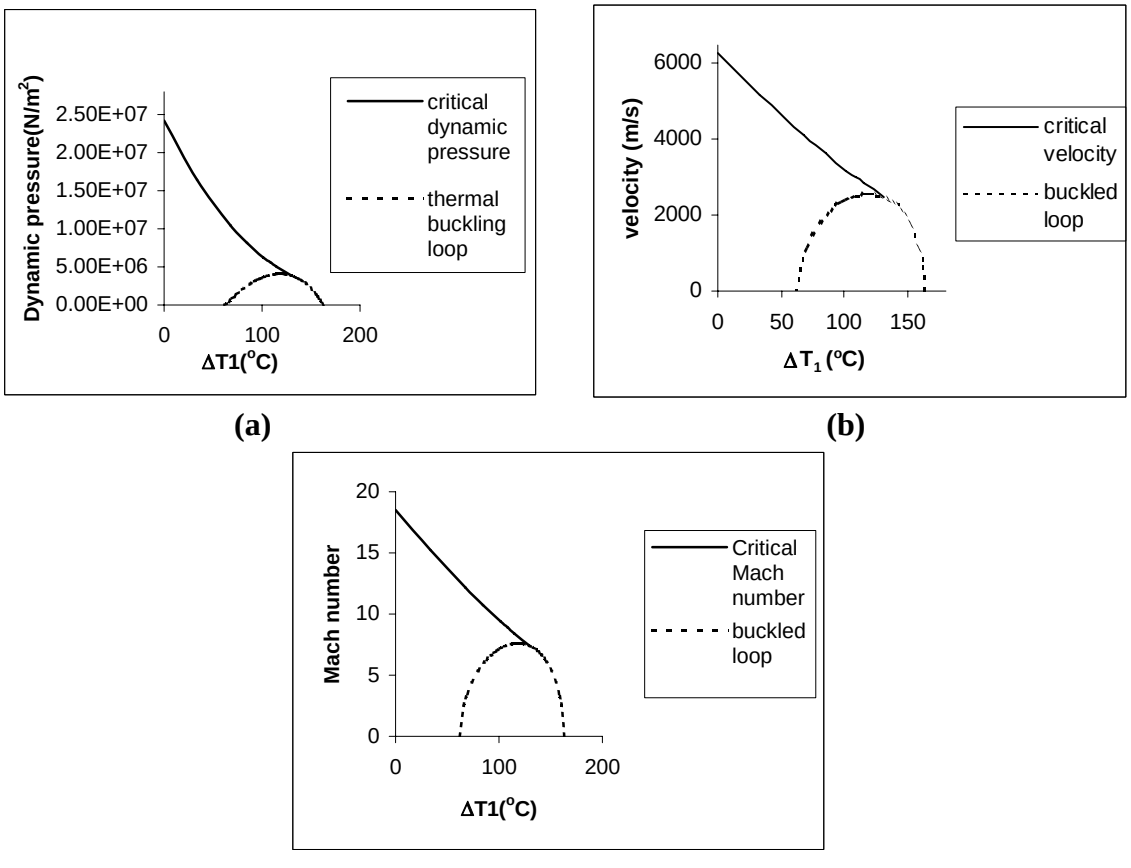

Fig 5.1 Variation of Critical Parameters due to parabolic temperature distribution over the square aluminium panel (specimen A). Flow along edge *a*.
Air Density assumed is 1.225 *kg/m*^{3}.
a) Critical Dynamic pressure b) Critical Velocity c) Critical Mach number

5.2.2 Effect of flow direction and thermal profile with arbitrary flow direction

The variation of critical parameters (critical dynamic pressure, critical velocity, critical Mach number) for the given square panel is investigated. The results are presented in Table 5.1. The graphical representation of the variation of critical parameters for the panel with flow angle is presented in Fig 5.2.

Table 5.1.a Variation of Critical Dynamic pressure with various parabolic temperature profile and flow angle.

	Critical Dynamic Pressure (N/m^2)				
	$\theta = 0^o$	$\theta = 30^o$	$\theta = 45^0$	$\theta = 60^o$	$\theta = 90^o$
$\Delta T_1 = 0$	2421017.88	25188342.96	25567121.59	25188342.96	2421017.88
$\Delta T_1 = 34.524$	16423184.76	17014836.98	17238392.78	17014836.98	16423184.76
$\Delta T_1 = 86.31$	8163103.168	8385589.371	8464159.93	8385589.371	8163103.168
$\Delta T_1 = 133.26$	3879313.753	3952387.114	3979477.351	3952387.114	3879313.753

Table 5.1.b Variation of Critical velocity with various parabolic temperature profile and flow angle.

	Critical Velocity (*m/s*)				
	$\theta = 0^o$	$\theta = 30^o$	$\theta = 45^0$	$\theta = 60^o$	$\theta = 90^o$
$\Delta T_1 = 0$	6287.145	6412.786	6460.82	6412.786	6287.145
$\Delta T_1 = 34.524$	5178.162	5270.61	5305.121	5270.61	5178.162
$\Delta T_1 = 86.31$	3650.69	3700.102	3717.396	3700.102	3650.69
$\Delta T_1 = 133.26$	2516.66	2540.25	2548.94	2540.25	2516.66

Table 5.1.c Variation of Critical Mach number with various parabolic temperature profile and flow angle.

	Critical Mach number				
	$\theta = 0^o$	$\theta = 30^o$	$\theta = 45^0$	$\theta = 60^o$	$\theta = 90^o$
$\Delta T_1 = 0$	18.492	18.86	19.002	18.86	18.492
$\Delta T_1 = 34.524$	15.23	15.5	15.6	15.5	15.23
$\Delta T_1 = 86.31$	10.74	10.88	10.93	10.88	10.74
$\Delta T_1 = 133.26$	7.41	7.47	7.5	7.47	7.41

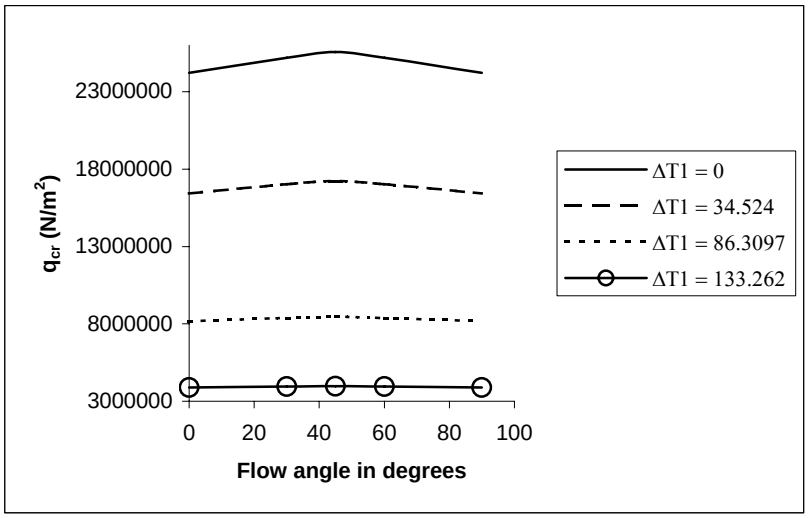

(a)

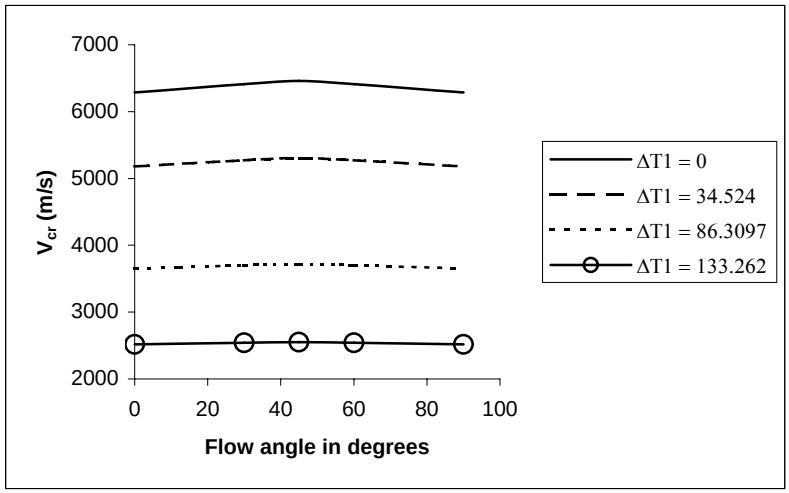

(b)

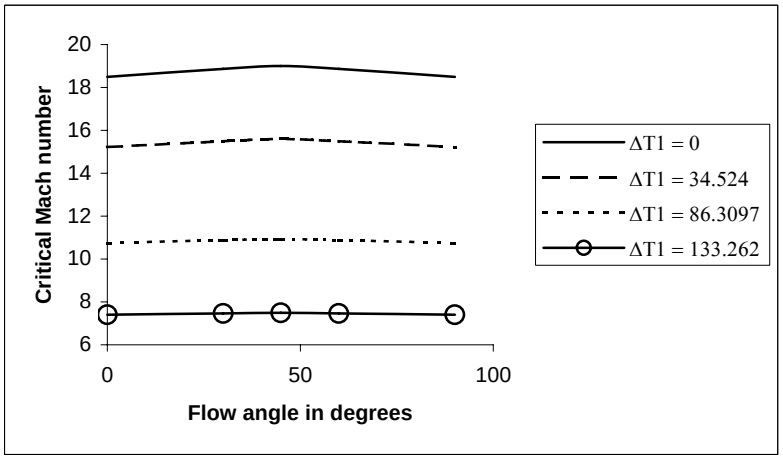

(c)

Fig 5.2 Variation of Critical Parameters for various flow angle with parabolic temperature distribution over square panel a) Critical Dynamic pressure b) Critical Velocity c) Critical Mach number. Air Density assumed is 1.225 *kg/m^3*.

5.2.3 Effect of Uniform Edge Loading due to edge constraint on thermal expansion on the flutter boundary of the panel with flow along x-direction.

In-plane edge loading per unit edge length, N_{xo} and N_{yo} on the panel can develop from the in-plane edge constraints to thermal expansion. Panels with immovable hinged supports can generate such edge loads. For specimen A, these edge loads (per unit edge length) from edge constraints to thermal expansion, as given in equation (2.21) can be expressed as

$$N_{xo} = N_{yo} = \frac{E}{(1-\mu)}\alpha(\Delta T_2)h \quad = 5336\Delta T_2$$

Here the effective panel temperature ΔT_2 for edge loads is defined as in equations (2.22) and (2.24)

$$\Delta T_2 = T_{mean} - T_{reference} = T_{edge} + \frac{4}{9}\Delta T_1 - T_{reference}$$

These edge loads vanish at the reference temperature.

The effects of edge loading from in-plane edge constraints on thermal expansion upon the critical dynamic pressure is demonstrated for the given square panel. Variation of critical parameters (critical dynamic pressure, critical velocity, critical Mach number) due to the effects of edge loading from in-plane edge constraints on thermal expansion associated with a parabolic temperature distribution over the given square panel is shown in Fig.5.3. The results are plotted for different temperatures ΔT_2 that generate the edge loads. It must be noted that these results are generated by taking the *net* in-plane loads (N_x, N_y, N_{xy}) as given in equation (2.4), i.e. the contributions of the in-plane stress resultants (N_{xT}, N_{yT}, N_{xyT}) from the parabolic profile are superposed with those from the edge loads (N_{x0}, N_{y0}).

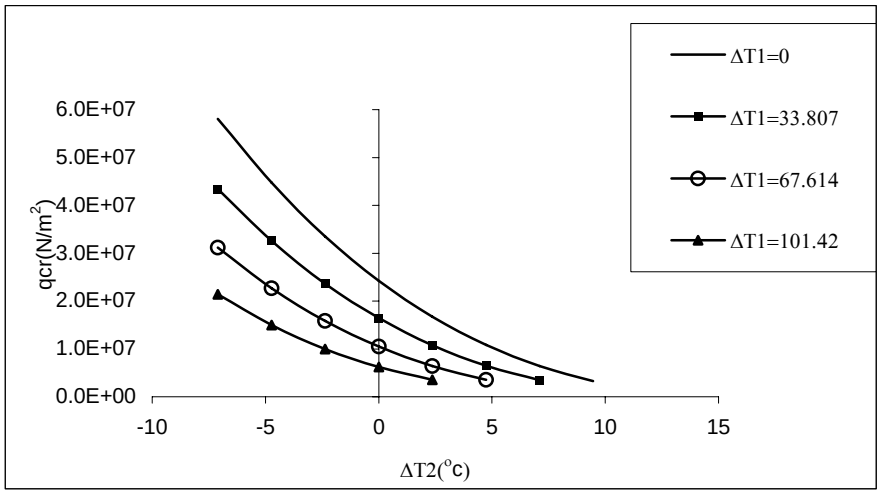

(a)

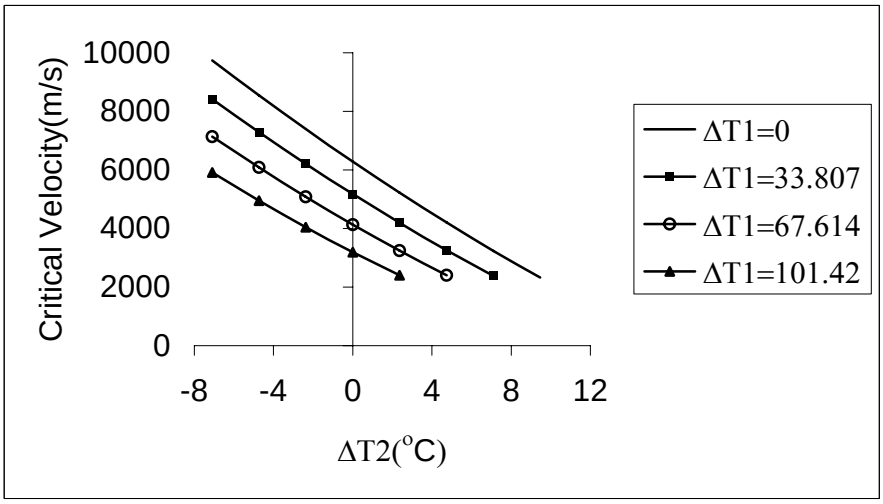

(b)

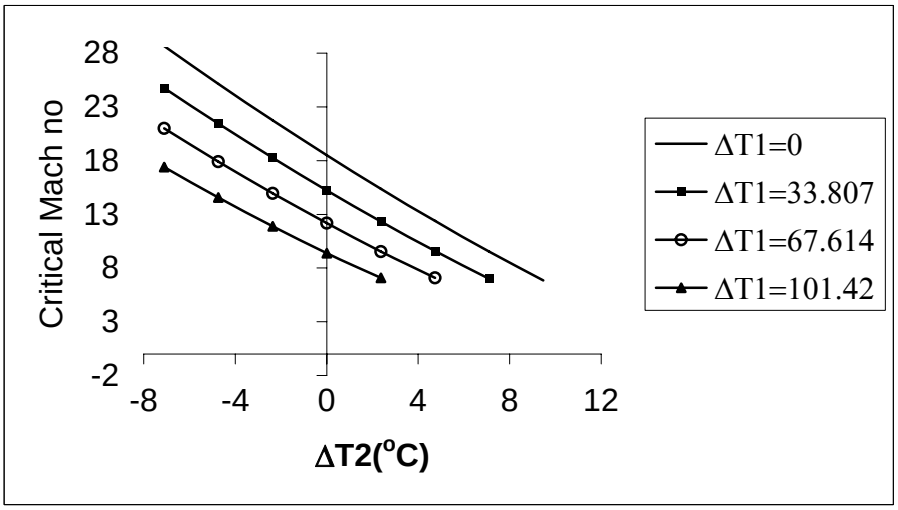

(c)

Fig 5.3 Variation of Critical parameters for Specimen A with the effects of edge loading from in-plane edge constraints on thermal expansion. Flow along *x*-direction (edge *a*). Air Density assumed is 1.225 kg/m^3.

a) Critical dynamic pressure b) Critical velocity c) Critical Mach number.

5.2.4 Effect of Uniform Edge Loading due to edge constraint on thermal expansion on Flutter Boundary of the panel with arbitrary flow direction

The variation of critical Mach number due to effects of various temperatures ΔT_2 that generate edge loading from in-plane edge constraints on thermal expansion over the panel when the panel is subjected to arbitrary flow direction are presented in Fig 5.4. Fig 5.4a shows the results for flow angle of $\theta = 30^0$. For a square panel the results are same for $\theta = 30^0$ and $\theta = 60^0$. Figs 5.4b shows the results for flow angle of $\theta = 45^0$.

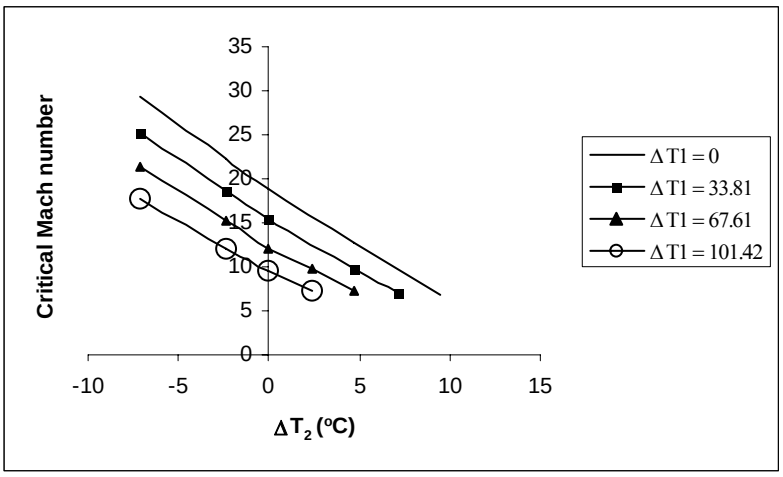

(a)

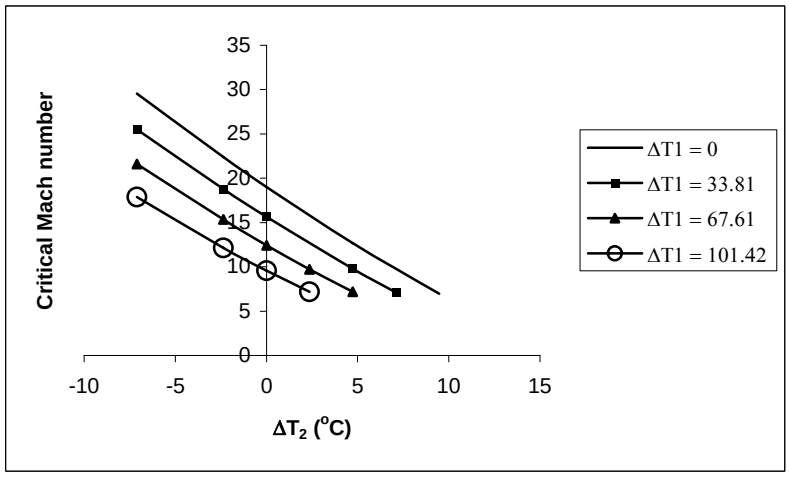

(b)

Fig 5.4 Variation of Critical Mach number for Specimen A with the effects of edge loading from in-plane edge constraints on thermal expansion for flow angle of a) $\theta = 30^0$ **& b)** $\theta = 45^0$ **. Air Density assumed is 1.225** ***kg/m*** ^{3}**.**

5.3. Numerical Results for the square panel (Specimen A) using NASTRAN:

For the square plate (specimen A; $0.25m \times 0.25m$) the critical parameters are calculated with the finite element package NASTRAN for no thermal condition and flow along *x*-direction. The entire square panel is discretized into 10x10=100 elements. The finite element mesh of the panel is presented in Fig 5.5.

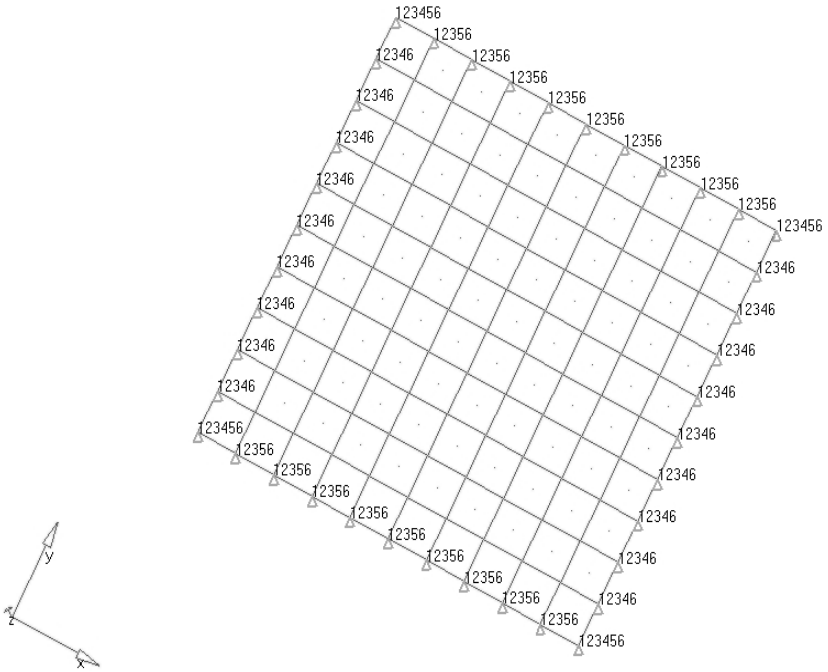

Fig 5.5 Finite element model for square panel

The free vibration characteristics (natural frequencies) are given in Table 5.2.a. The critical parameters (dynamic pressure, velocity and Mach number) are determined and compared with the corresponding analytical results. These results are presented in Table 5.2 b.

Table 5.2.a Natural frequency of the square panel

Mode (m, n)	Natural Frequency (*Hz*)	
	Analytical	NASTRAN
(1,1)	177.5933	175.16
(2,1)	443.9832	435.14
(3,1)	887.9664	870.35
(1,2)	443.9832	435.14
(2,2)	710.3731	677.95
(3,2)	1154.356	1089.5
(1,3)	887.9664	870.35
(2,3)	1154.356	1089.5
(3,3)	1509.543	1482.11

Table 5.2.b Comparison of analytical results with NASTRAN for the square panel (Specimen A) with flow along edge '*a*'. (Air density is 1.225 kg/m^3).

	Critical Dynamic Pressure q_{cr} (Pa)	Critical Flow Speed V_{cr} (m/s)	Critical Mach number M_{cr}
Analytical	2421017.88	6287.145	18.492
NASTRAN	23430712.81	6185	18.19

5.4. Numerical Results for a panel of aspect ratio = 7.2 (Specimen B) using theoretical formulation

The aluminium panel of aspect ratio 7.2 (which is typical of a wing panel of a supersonic re-entry vehicle) is considered here. Assumed air density is 0.715 kg/m^3 (corresponding to a dynamic pressure of 50 *KPa).*

The dimensions and properties of the panel are as follows:

Length of panel, a = $0.36m$
Width of panel, b = $0.05m$
Aspect ratio, a/b = 7.2
Thickness of panel, h = $0.0011m$
Material of panel = Aluminium
Modulus of Elasticity, E = $70\text{x}10^9\ N/m^2$
Poisson's ratio, μ = 0.3
Coefficient of thermal expansion of Aluminium
α = $2.3\text{x}10^{-5}/^oC$
Density of material, ρ_{mat} = $2764\ kg/m^3$
Density of air, ρ_{air} = $0.715\ kg/m^3$
Dynamic pressure parameter

$$\lambda = \frac{2qa^3}{D\sqrt{M^2-1}} = \frac{0.00391v^2}{\sqrt{\left(\frac{v}{340}\right)^2-1}}$$

$$\psi = \frac{\alpha Eha^2\Delta T_1}{\pi^2 D} = 2.4778\Delta T_1$$

$$N_{xo} = N_{yo} = \frac{E}{(1-\mu)}\alpha(\Delta T_2)h = 2530\Delta T_2$$

For the given plate specimen B, critical velocity values are calculated for various parabolic temperature profiles (ΔT_1). The variation of critical parameters (critical dynamic pressure, critical velocity, critical Mach number) for this specimen B with flow along *x*-direction are shown in Fig 5.6.

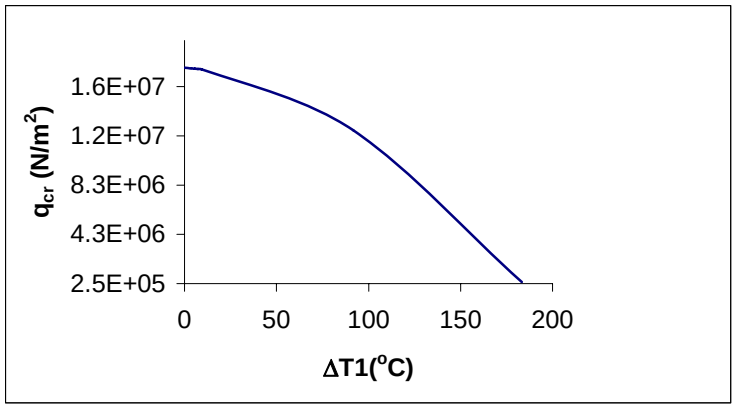

(a)

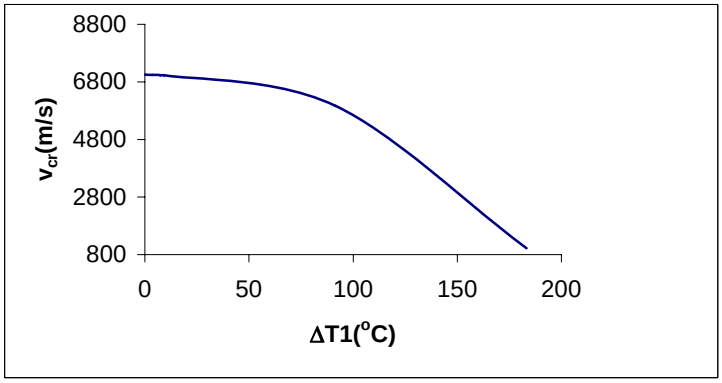

(b)

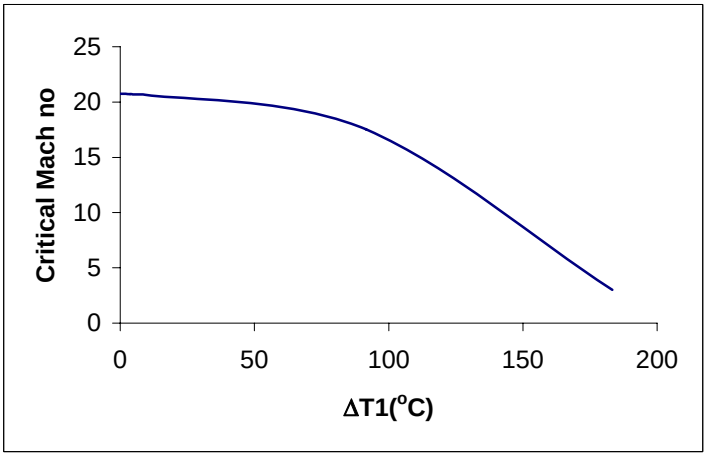

(c)

Fig 5.6 Variation of Critical parameters due to parabolic temperature distribution for the panel of aspect ratio *a/b*=7.2 (Specimen B). Flow along x-direction (edge *a*). a) Critical dynamic pressure b) Critical velocity c) Critical Mach number. Air density assumed 0.715 *kg/m*^{3}.

The effect of flow direction on these critical parameters is also investigated. The results are presented in Table 5.3. The results are graphically presented in Fig 5.7.

Table 5.3.a Variation of Critical Dynamic Pressure (for specimen B) with various parabolic temperature profiles and flow angles.

	Critical Dynamic pressure (N/m^2)			
	$\theta = 0^o$	$\theta = 30^o$	$\theta = 45^0$	$\theta = 60^o$
$\Delta T_1 = 0$	17786384	23686262.99	35426862.34	70180191.91
$\Delta T_1 = 35.65$	17448063.93	23237078.31	34760355.47	68874679.96
$\Delta T_1 = 146.61$	2507478.86	3350547.483	5021926.04	9942181.482

Table 5.3.b Variation of Critical Velocity (for specimen B) with various parabolic temperature profiles and flow angles.

	Critical velocity (m/s)			
	$\theta = 0^o$	$\theta = 30^o$	$\theta = 45^0$	$\theta = 60^o$
$\Delta T_1 = 0$	7053.519	8139.74	9954.71	14011.004
$\Delta T_1 = 35.65$	6986.112	8062.18	9860.62	13880.07
$\Delta T_1 = 146.61$	2648.38	3061.4	3747.98	5273.55

Table 5.3.c Variation of Critical Mach number (for specimen B) with various parabolic temperature profiles and flow angles.

	Critical Mach number			
	$\theta = 0^o$	$\theta = 30^o$	$\theta = 45^0$	$\theta = 60^o$
$\Delta T_1 = 0$	20.75	23.94	29.28	41.21
$\Delta T_1 = 35.65$	20.55	23.71	29.002	40.82
$\Delta T_1 = 146.61$	7.79	9.004	11.023	15.51

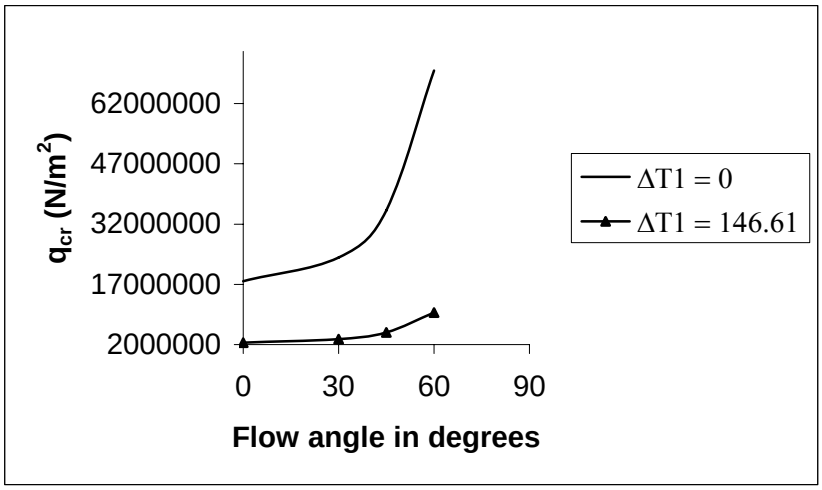

(a)

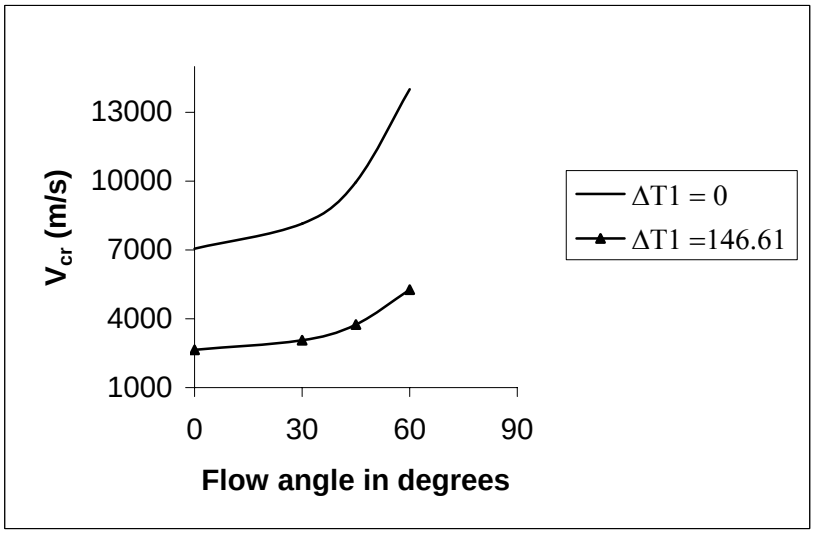

(b)

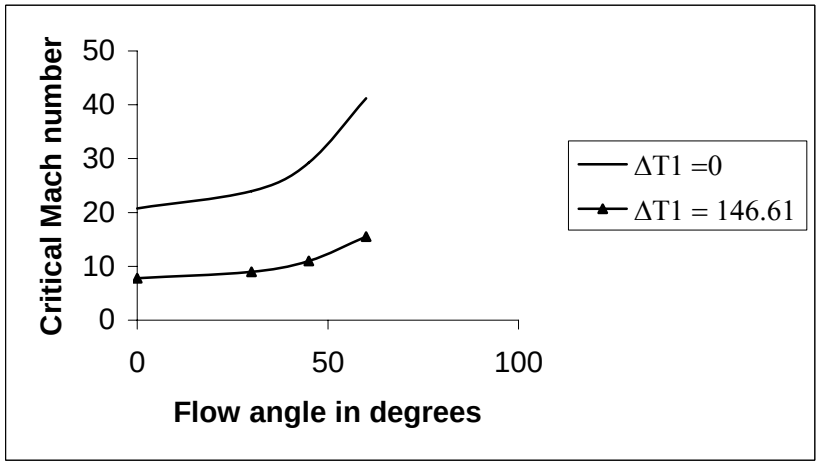

(c)

Fig 5.7 Variation of critical parameters for various flow angles with parabolic temperature distribution over panel of aspect ratio =7.2 (Specimen B). Air density assumed *0.715 kg/m^3*.
a) Critical dynamic pressure b) Critical velocity c) Critical Mach number

Effect of edge loading, in terms of the temperature ΔT_2 from in-plane edge constraints on thermal expansion over the given panel (specimen B) is shown in Fig.5.8. Flow is along *x*-direction (edge *a*). Air density is assumed to be 0.715 kg/m^3.

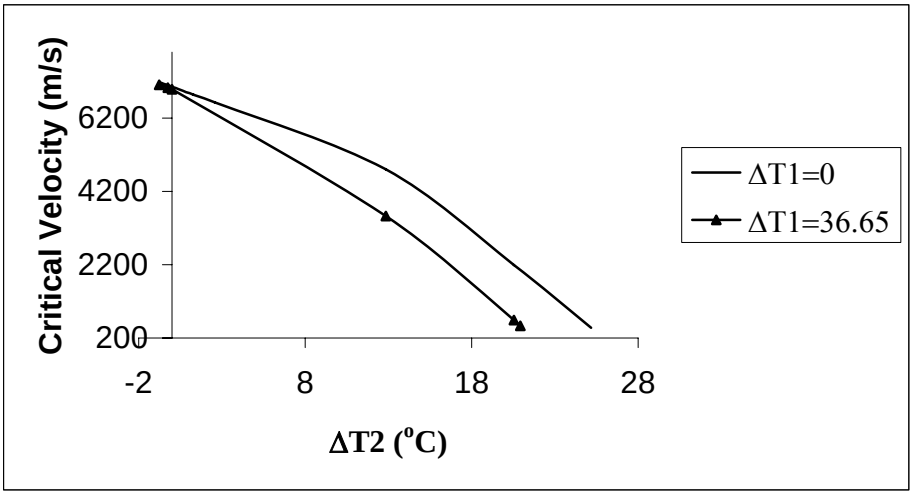

(a)

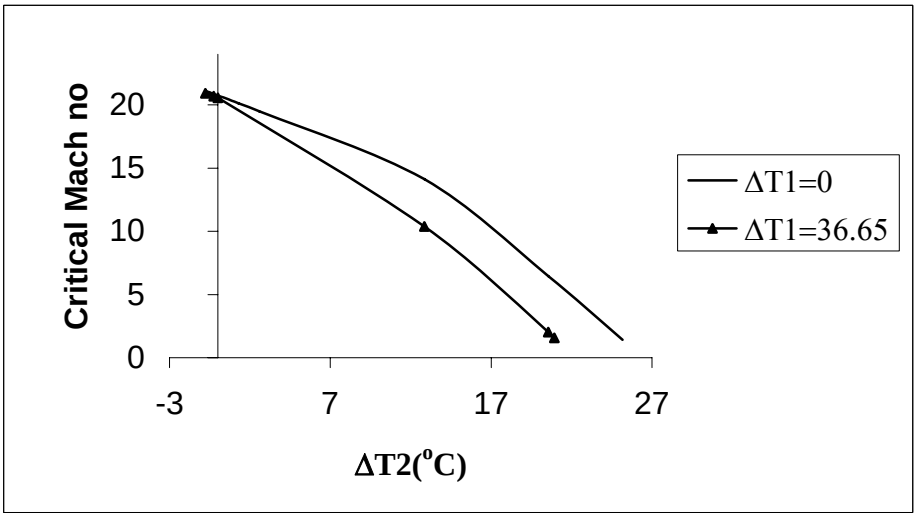

(b)

Fig 5.8 Variation of Critical parameters for Specimen B with the effects of edge loading from in-plane edge constraints on thermal expansion. Flow along *x*-direction (edge *a*). Air Density assumed is 0.715 kg/m^3.
a) Critical velocity b) Critical Mach number.

The effect on flow direction on the variation of critical Mach number has been investigated also for specimen B. Results with three flow directions and various temperatures ΔT_2 that generate edge loading from in-plane edge constraints (for specimen B) are presented in Fig 5.9.

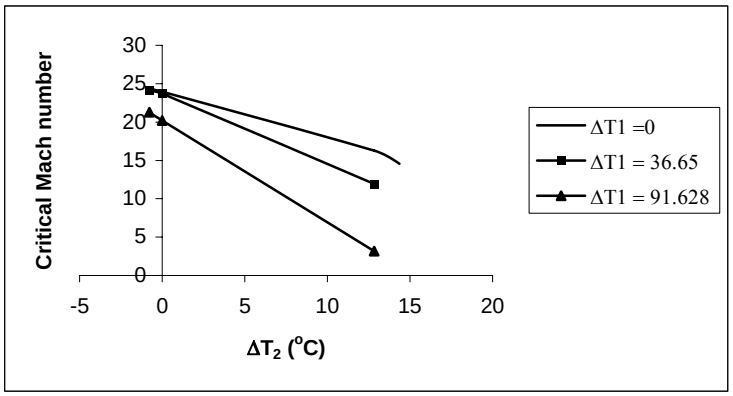

(a)

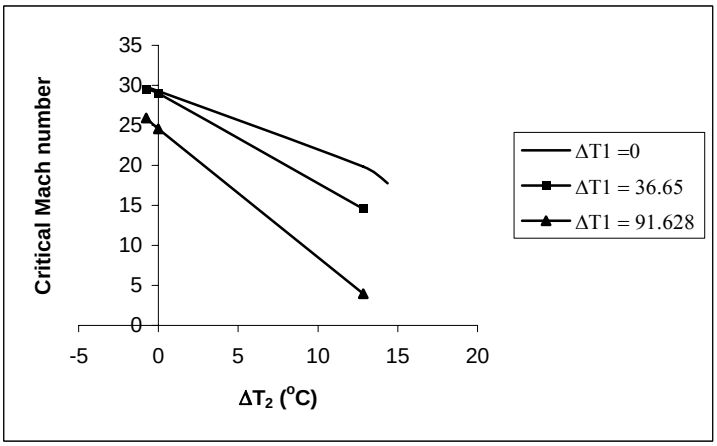

(b)

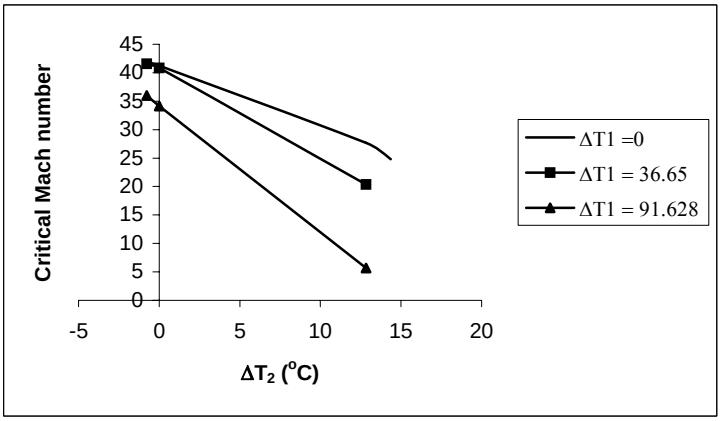

(c)

Fig 5.9 Variation of Critical Mach number for Specimen B with the effects of edge loading from in-plane edge constraints on thermal expansion for flow angle of a) $\theta = 30^0$ **& b)** $\theta = 45^0$ **. Air Density assumed is 0.715** ***kg/m*** ^{3} **.**

5.5 Numerical Results for a panel of aspect ratio=7.2 (specimen B) using NASTRAN

For the specimen B ($0.36m \times 0.05m$), the critical parameters (critical dynamic pressure, critical flow speed, critical Mach number) are calculated with the finite element package NASTRAN for no thermal condition and flow along x-direction. The entire panel is discretized into 10x10=100 elements. The finite element mesh is displayed in Fig 5.10.

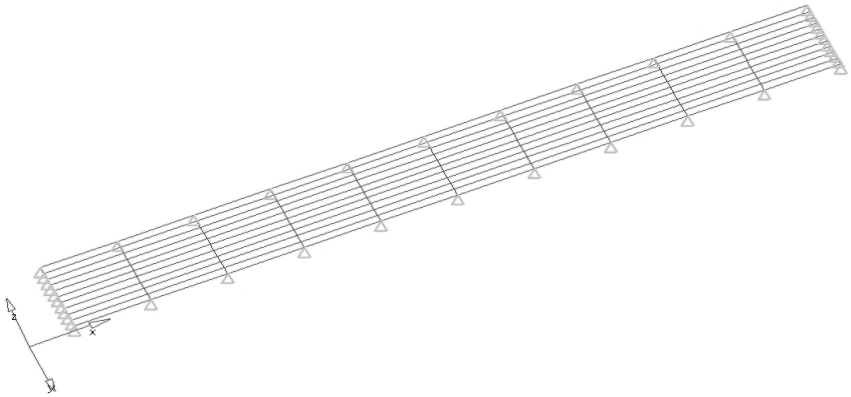

Fig 5.10 Finite element model for panel of aspect ratio = 7.2

The free vibration characteristics (natural frequencies) are given in Table 5.4.a. The critical parameters (dynamic pressure, velocity and Mach number) are determined and compared with the corresponding analytical results. These results are presented in Table 5.4 b.

Table 5.4.a Natural frequency of the Rectangular panel of aspect ratio =7.2

Mode (m, n)	Natural Frequency (Hz)	
	Analytical	NASTRAN
(1,1)	1073	1061.52
(2,1)	1134	1090.95
(3,1)	1235	1141.41
(1,2)	4230	4045.73
(2,2)	4291	4127.29
(3,2)	4393	4179.79
(1,3)	9493	8866.82
(2,3)	9554	9159.17
(3,3)	9656	9342.3

Table 5.4.b Comparison of analytical results with NASTRAN for a panel of aspect ratio *a/b* = 7.2 with air flow along edge '*a*'.

	Critical Dynamic Pressure q_{cr} (Pa)	Critical Flow Speed V_{cr} (m/s)	Critical Mach number M_{cr}
Analytical	17786384.34	7053.52	20.75
NASTRAN	17035378.72	6903	20.30

5.6 Chapter Summary and Observations

A numerical study of the supersonic flutter boundary of panels of given dimension and material properties is made. The variation of critical parameters (flutter dynamic pressure/ flutter velocity) with parabolic temperature distribution over the panel along with the effect of Uniform Edge Loading on Flutter Boundary of the panel is generated.

The results reveal that there is dramatic reduction in the critical Mach number due to the parabolic thermal profile even for panels that are simply supported at the edges (without in-plane edge constraints). From Fig 5.1, one can observe that for the given simply supported square panel (specimen A) a parabolic temperature profile parameter ΔT_1=130.5 ^{0}C causes 60.27% reduction in critical Mach number, for flows along *x*-direction (edge *a*). Beyond this thermal condition, divergence sets in. From Fig 5.3, it can be observed that further reduction of the critical Mach number occurs from the temperature parameter ΔT_2 because of edge constraints to thermal expansion). From Figs 5.2 and 5.4, it is evident that the least of the critical Mach number occurs at a flow parallel to one of the edges, and the maximum occurs for a flow at 45^0 with the edge, for any thermal profile or edge constraints to thermal expansion.

Similar observations have been made with specimen B, of aspect ratio 7.2. From Fig 5.6, one can observe that for this given simply supported panel a parabolic temperature profile parameter ΔT_1=183.25^{0}C causes 85.45% reduction in critical Mach number, for flows along *x*-direction (edge *a*). Beyond this thermal condition, divergence sets in. From Fig 5.8, it can be observed that further reduction of the critical Mach number occurs from the temperature parameter ΔT_2 because of edge constraints to thermal expansion. From Figs 5.7 and 5.9, it is evident that the least of the critical Mach number occurs at a flow parallel to longer of two edges.

The results are validated for no thermal condition with finite element software NASTRAN. Good agreement between the results can be observed.

CHAPTER 6

CONCLUSION AND SCOPE FOR FUTURE WORK

6.1 Conclusion

The flutter behavior of panel exposed to supersonic airflow in arbitrary direction, in-plane load due to thermal expansion and parabolic temperature distribution over the panel has been studied theoretically. The theoretical results are validated with the finite element software package NASTRAN for no thermal condition and flow along *x*-direction. From the results obtained the following conclusions are made:

1. The investigation of the effect of flow angularity on the critical dynamic pressure for panels of various aspect ratios reveals that the dynamic pressure decreases as the flow gets more and more aligned to the longest direction. This implies that the flow along the longer side is most critical. *i.e.* the dynamic pressure is lowest for this direction.

2. Investigation reveals adverse thermal effects on supersonic flutter boundary through significant fall in critical dynamic pressure/flow velocity, due to
   a) Parabolic temperature profile
   b) Compressive in-plane load arise due to in-plane edge constraints to thermal expansion of the plate.

3. It can be observed that for a given temperature profile the critical dynamic pressure falls as the flow tends towards the longer direction of the panel. Also, for a given flow direction and given aspect ratio, the value of critical dynamic pressure falls with temperature. Thus one can conclude that both thermal conditions and flow direction affect the flutter boundary

4. Good agreement between NASTRAN result and theoretical results for the flow along x-direction with no thermal conditions is observed.

6.2. Scope for future work

- The present work is limited to in-plane compression effects from thermal influence, with no temperature gradients. Real panels in the RLV are actually subjected to extreme temperature gradients across panel thickness. The present method of analysis can be extended to study such cases by incorporating suitable terms that represent effects of such harsh temperature gradients.

- In future work the temperature dependant material properties can be considered.

- Presently, the thermal conditions are simulated with analytical tools only. It can be extended to simulate thermal conditions also in the NASTRAN models, through generation of appropriate in-plane forces and edge forces.

REFERENCES

1. **Fung.Y.C.,** (1955), *"Introduction to Aeroelasticity"*, John Willey and sons, Newyork.

2. **Bisplinghoff.R.L and Ashley.H.,** (1962) *"Principles of Aeroelasticity"*, Willey, Newyork.

3. **Lanchester, F.W.** (1916) *"Torsional Vibration of an Aeroplane"*, Aeronatutical Research Committee, R&M.276, Part1.

4. **Bairstow. L and Fage,A.** (1916) *"Oscillations of the Tail Plane and Body of an Aeroplane in Flight"*, Aeronautical Research Committee, R&M.276, Part2.

5. **Holt Ashley and Garabed Zartarian.** (1956) ***"****Piston theory - a new aerodynamic tool for the aeroelatican"*. Journal of the Aeronautical Sciences, vol.23, pg.1109-1118.

6. **Fung,Y.C.B.,** (1960) *"A summary of the theories and Experiments on panel flutter"*. AFOSR TN. 60-224.

7. **Herman L. Bohon and Sidney C. Dixon** (1964) *"Some Recent Developments in Flutter of Flat Panels"*, Journal of Aircraft, vol.1, pg.280-288.

8. **Hedgepeth, John M.,** (1957) *"Flutter of rectangular simply supported panels at high supersonic speeds"*, Journal of Aeronautical Sciences, vol.24, No 8, pg. 563-573.

9. **Fralich,R.W.,** (1965) "*Post buckling Effects on the Flutter of Simply Supported* Rectangular panels at Supersonic Speeds", NASA TN-D-1615.

10. **Ellen, C.H.** (1965) *"Approximate Solutions of Membrane Flutter Problem"*, AIAA Journal, vol.3, pg. 1186-1193.

11. **G.Sander, C.Bon and M.Geradin** (1973) *"Finite element analysis of supersonic panel flutter"*, International Journal for Numerical Methods in Engineering, vol.7, pg.379-394.

12. **Harry G. Schaeffer and Walter L. Heard** (1965) "*Supersonic Flutter of a Thermally Stressed Flat Panel with Uniform Edge loads", NASA* TN-D-3077.

13. **Larry L. Erickson** (1966) "*Supersonic Flutter of Flat Rectangular orthotropic Panels Elastically Restrained against Edge Rotation*", NASA TN-D-3500.

APPENDIX A

The integral resulting from the aerodynamic loading equation (2.15.a) gives the following expression:

$$(L_1)_{rs} = \frac{2}{\pi^4} \sum_{\substack{m=1 \\ m \neq r}}^{R} \frac{rma_{ms}\left[1-(-1)^{r+m}\right]}{r^2-m^2}$$

$$(L_2)_{rs} = \frac{2}{\pi^4} \sum_{\substack{n=1 \\ n \neq s}}^{S} \frac{sna_{rn}\left[1-(-1)^{s+n}\right]}{s^2-n^2}$$

The integrals $(I_1)_{rs}$, $(I_2)_{rs}$ and $(I_3)_{rs}$ given by equations (2.15.b),(2.15.c) and (2.15.d) are evaluated by making use of the specific definition of the stress function given by equation (2.5).

$$(I_1)_{rs} = -\frac{2C\alpha Eha^3\Delta T_1}{\pi^2 b} M_{rs}$$

$$(I_2)_{rs} = \frac{4C\alpha Eha^2\Delta T_1}{\pi^2} Q_{rs}$$

$$(I_3)_{rs} = -\frac{2C\alpha Ehab\Delta T_1}{\pi^2} P_{rs}$$

where

$$M_{rs} = \sum_{\substack{m=1 \\ m \neq r}}^{R} \sum_{\substack{n=1 \\ n \neq s}}^{S} a_{mn} \left\{ \frac{72m^2ns\left[(-1)^{n+s}+1\right]\left[(-1)^{m+r}+1\right]\left[(m+r)^4-(m+r)^4\right]}{\pi^4(n-s)^2(n+s)^2(m+r)^4(m-r)^4} \right\}$$

$$-\frac{12}{\pi^2}\left[\frac{(r\pi)^2}{60}+\frac{3}{4(r\pi)^2}\right]\sum_{\substack{n=1 \\ n \neq s}}^{S}\frac{ns\left[(-1)^{n+s}+1\right]a_{rn}}{(n-s)^2(n+s)^2} - \frac{9}{s^2\pi^4}\sum_{\substack{n=1 \\ n \neq s}}^{S}\frac{m^2\left[(-1)^{m+r}+1\right]\left[(m+r)^4-(m-r)^4\right]a_{ms}}{(m+r)^4(m-r)^4}$$

$$+\frac{3}{2}\left(\frac{r}{s}\right)^2\left[\frac{1}{60}+\frac{3}{4(r\pi)^4}\right]a_{rs}$$

$$P_{rs} = \sum_{\substack{m=1 \\ m\neq r}}^{R} \sum_{\substack{n=1 \\ n\neq s}}^{S} a_{mn} \left\{ \frac{72m^2 mr\left[(-1)^{m+r}+1\right]\left[(-1)^{n+s}+1\right]\left[(n+s)^4-(n-s)^4\right]}{\pi^4 (n-s)^4 (n+s)^4 (m+r)^2 (m-r)^2} \right\}$$

$$- \frac{12}{\pi^2}\left[\frac{(s\pi)^2}{60} + \frac{3}{4(s\pi)^2} \right] \sum_{\substack{m=1 \\ n\neq r}}^{R} \frac{mr\left[(-1)^{m+r}+1\right] a_{ms}}{(m-r)^2 (m+r)^2} - \frac{9}{r^2\pi^4} \sum_{\substack{n=1 \\ n\neq s}}^{S} \frac{n^2\left[(-1)^{n+s}+1\right]\left[(n+s)^4-(n-s)^4\right] a_{rn}}{(n+s)^4 (n-s)^4}$$

$$+ \frac{3}{2}\left(\frac{s}{r}\right)^2 \left[\frac{1}{60} + \frac{3}{4(s\pi)^4} \right] a_{rs}$$

$$Q_{rs} = \sum_{\substack{m=1 \\ m\neq r}}^{R} \sum_{\substack{n=1 \\ n\neq s}}^{S} \frac{9mn}{\pi^4} a_{mn}\left[(-1)^{n+s}+1\right]\left[(-1)^{m+r}+1\right] \times \left\{ \left[\frac{(s-n)^3+(s+n)^3}{(s-n)^3(s+n)^3} \right] \left[\frac{(r-m)^3+(r+m)^3}{(r+m)^3(r-m)^3} \right] \right\}$$

$$+ \frac{9}{4\pi^4 s^2} \sum_{\substack{m=1 \\ m\neq r}}^{R} m\left[(-1)^{m+r}+1\right] \left[\frac{(r-m)^3+(r+m)^3}{(r-m)^3+(r+m)^3} \right] a_{ms}$$

$$+ \frac{9}{4\pi^4 r^2} \sum_{\substack{n=1 \\ n\neq s}}^{S} n\left[(-1)^{n+s}+1\right] \left[\frac{(s-n)^3+(s+n)^3}{(s-n)^3+(s+n)^3} \right] a_{rn} + \frac{9}{16\pi^4 r^2 s^2} a_{rs}$$

DOCUMENTATION SHEET

	NATIONAL AEROSPACE LABORATORIES	**Class : Restricted** **No. of Copies : 20**

Title : Analytical investigation of Supersonic Panel Flutter under Thermal Environment with Arbitrary Flow Direction

Author / s : Somenath Mukherjee, Deepa N, Avinash R. , M. Manjuprasad, S. Viswanath

Division : Structures				**NAL Project No. :** S – 0 - 249			
Document No. : PD-ST-0704				**Date of Issue** : March 2007			
Contents	59	**Pages**	38	**Figures**	12	**Tables**	13	**References**

External Participation : -

Sponsor : VSSC (ISRO)

Approval : Head, Structures Division S Somanath 26/04/07

Remarks :

Keywords : Supersonic Panel Flutter, Critical Dynamic Pressure, Flutter Speed, Thermal Profile, Aspect Ratio, Flow Direction, In-plane Loads.

Abstract:

Panels and Thermal Protection System of re-entry vehicles are subjected to a wide range of flow condition during ascent and reentry phases. The flow can vary from subsonic continuum flow to hypersonic rarefied flow with wide ranging dynamic pressure and associated aerodynamic heating. One of the main design considerations is the assurance of panel safety against panel flutter under the flow conditions characterized by harsh thermal environment. The objectives of this work are to understand the physical principles behind panel flutter under supersonic flow with arbitrary flow angles and given thermal profiles, to make an estimate of the lowering of the critical dynamic pressure (flutter boundary) of the panels due to high thermal distributions in the restrained panels. Using analytical techniques, a mathematical formulation has been developed which can predict flutter boundaries under parabolic distribution of temperature, in addition to the flat temperature profile, over the panels.

The piston theory is used for aerodynamic pressure computations. Studies have been carried out for rectangular panels of various aspect ratios subjected to flat and parabolic type thermal profiles and various flow directions (restricted on the plane of the panels). The theoretical results are validated with the finite element software package NASTRAN for no thermal condition and flow along x-direction. It has been observed that the flutter boundaries fall sharply with temperature, indicating that a careful study of the actual panels of the vehicle under the anticipated thermal profiles is necessary for design purpose. Furthermore, it has been observed that for any rectangular panel, flow along the longer side is most critical.